26

Imaging Strain Fields

CHAPTER PREVIEW

As we discussed in Chapter 24, bending of the lattice planes causes a change in the diffraction conditions and therefore a change in the contrast of the image. The presence of a lattice defect in the specimen causes the planes to bend close to the defect. The special feature here is that the bending varies not just laterally, but also through the specimen. Since the details of the bending generally depend on the characteristics of the defect, we can learn about the defect by studying the contrast in the TEM image. This simple principle has led to one of the main applications of TEM, namely, the study of defects in crystalline materials. We can claim that our understanding of the whole field of dislocations and interfaces, for example, has advanced because of TEM. We have even discovered new defects using TEM—like the stacking-fault tetrahedron, the faulted dipole, and the multipole.

Usually we want to learn two things about these defects: we want to know where they are and then understand what they are. So the idea underlying this chapter is the same as for bend contours: we use different reflections corresponding to different sets of lattice planes. We see how the defects affect the image contrast from those different lattice planes and thus characterize the defects. In case you are worried, we would like to emphasize that this is *not* a chapter about defects; it is concerned with understanding contrast in the TEM. We will introduce the necessary terminology and notation concerning defects, but we won't try to give you a comprehensive discussion of them. You should consult the standard references on dislocations at the end of the chapter if you need more details. However, we will show lots of pictures because now we are concerned with the appearance of images. We finish with some discussion of image simulation.

26.1 WHY IMAGE STRAIN FIELDS?

First, we should review our terminology. When we displace the atom at position **r** a distance **R**(**r**) from its site in the perfect crystal, we say the crystal is under a strain (ε). If the crystal is strained, then it must be subject to a stress which we'll call σ. (Metallurgists traditionally use these symbols and although σ means 'cross section' to a microscopist, we'll stick with it.) Since **R**(**r**) varies with position in the crystal, ε and σ will in general also vary with **r**. We will assume that ε and σ can each be defined at a point. Then we will refer to these quantities as the displacement field, **R**(**r**), the strain field, ε(**r**), and the stress field, σ(**r**). You will notice that these terms are used interchangeably in the literature although there is a clear causal sequence. What we image is the effect of the **R**(**r**).

To have an intuitive feel for why we see contrast from dislocations, consider the geometry shown in Figure 26.1. The diffraction geometry has been set up so that the specimen is slightly tilted away from the Bragg condition. The distortion due to the dislocation will then bend the near-diffracting planes back into the Bragg-diffracting condition. We have relrods so there will still be some intensity in the electron beam even when we are not at the exact Bragg condition. The figure shows planes bending at a dislocation; compare this to Figure 24.7 showing bend contours. Regions far from the dislocation are tilted well away from the Bragg condition, while the regions or either side of the dislocation core are at the Bragg condition for $\pm\mathbf{g}_{hkl}$. It is more difficult to recognize the diffracting planes for a screw dislocation (Figure 26.2) but the planes are bending just the same.

When studying a particular dislocation (edge or screw), we want to determine the following parameters

- The direction and magnitude of the Burgers vector, **b**, which is normal to the *hkl* diffracting planes (Figures 26.1 and 26.2B).

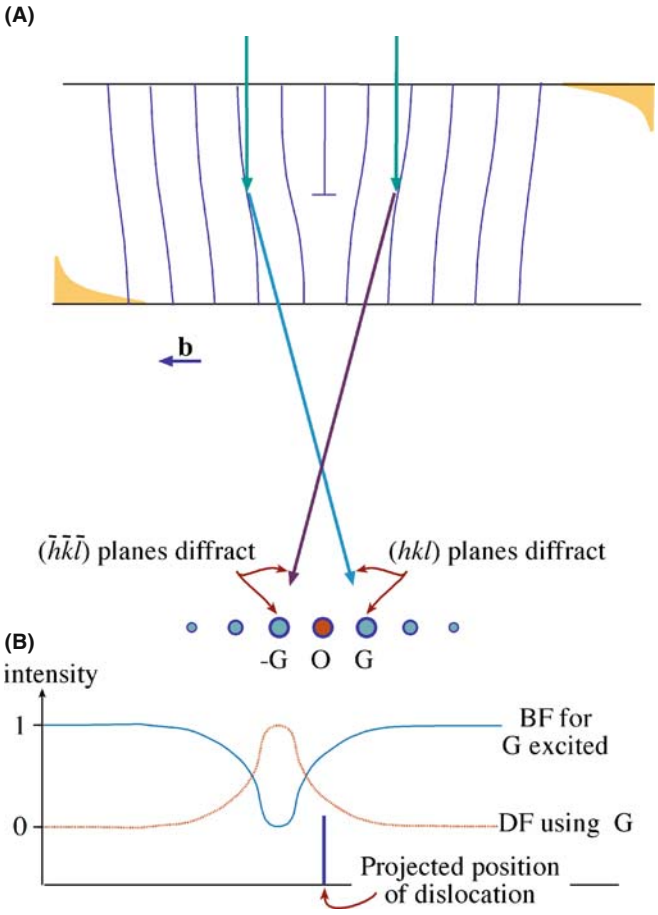

FIGURE 26.1. (A) The specimen is tilted slightly away from the Bragg condition ($\mathbf{s} \neq 0$). The distorted planes close to the edge dislocation are bent back into the Bragg-diffracting condition ($\mathbf{s} = 0$), diffracting into G and –G as shown. (B) Schematic profiles across the dislocation image showing that the defect contrast is displaced from the projected position of the defect. (As usual for an edge dislocation, **u** points into the paper.)

- The line direction, **u** (a vector), and therefore, the character of the dislocations (edge, screw, or mixed).
- The glide plane: the plane that contains both **b** and **u**.

There are other questions we want to answer

- Is the dislocation interacting with other dislocations, or with other lattice defects?
- Is the dislocation jogged, kinked, or straight?
- What is the density of dislocations in that region of the specimen (and what was it before we prepared the specimen)?
- Has the dislocation adopted some special configuration, such as a helix?

In many of these questions, you may find that stereomicroscopy or tomography (Section 29.1) can be very helpful although we will not emphasize those techniques here. The basic requirement if you do use stereomicroscopy is that you must form all of your images using the same **g** vector.

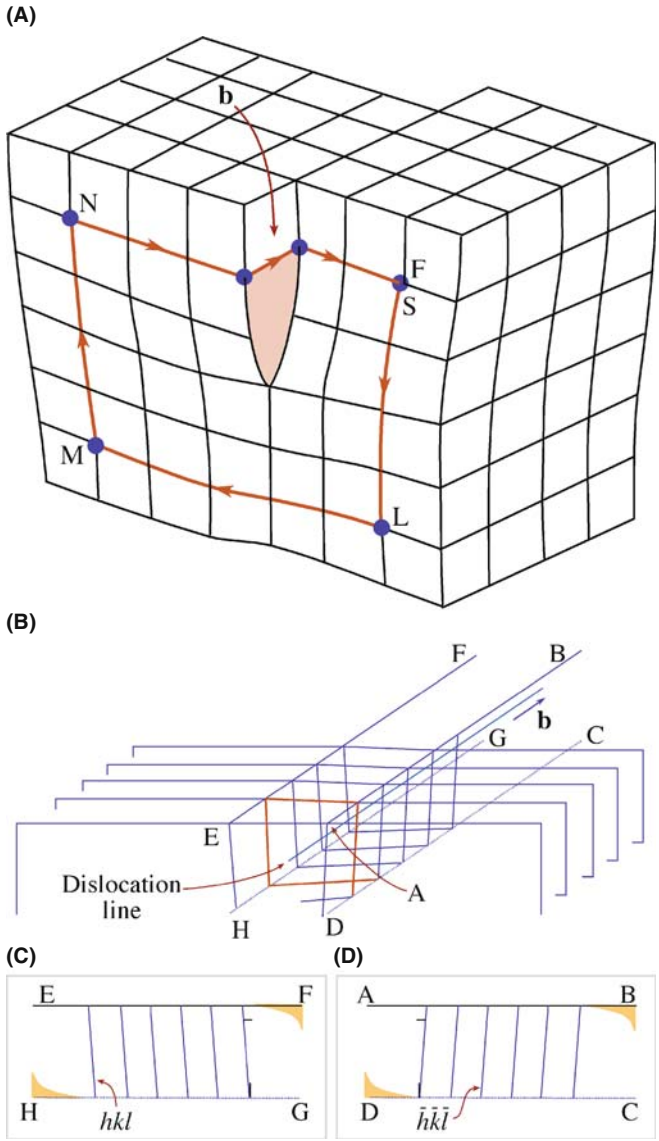

FIGURE 26.2. (A) Distortion of planes around a screw dislocation. The circuit SLMNF is used to define the Burgers vector, **b** (see Figure 26.5). (B) Schematic showing the rotation of the diffracting planes by a screw dislocation. The planes are rotated in opposite directions on either side of the dislocation. (C) and (D) show sections (ABCD and EFGH) through these diffraction planes.

26.2 HOWIE-WHELAN EQUATIONS

Let's start with the two-beam phenomenological approach because it worked so well in Chapter 25. An important assumption is that we have linear elasticity. What this means is that if we have $\mathbf{R}_1$ due to one defect and $\mathbf{R}_2$ due to a second defect, then at any point in the specimen we can just add these two values to determine the total displacement field, **R**. We will not consider anisotropic elasticity although this can readily be included in calculations if you're using a computer.

In Chapter 25, we showed that we could modify the Howie-Whelan equations to include a lattice distortion **R**. So for the imperfect crystal

$$\frac{d\phi_{\mathbf{g}}}{dz} = \frac{\pi i}{\xi_{\mathbf{0}}}\phi_{\mathbf{g}} + \frac{\pi i}{\xi_{\mathbf{g}}}\phi_{\mathbf{0}} \exp[-2\pi i(sz + \mathbf{g}.\mathbf{R})] \qquad (26.1)$$

Now we make a different substitution of variables (compare with equations 25.5 and 25.6). Set

$$\phi_{\mathbf{0}}(z)_{(\text{sub})} = \phi_{\mathbf{0}}(z) \exp\left(\frac{-\pi i z}{\xi_{\mathbf{0}}}\right) \qquad (26.2)$$

and

$$\phi_{\mathbf{g}}(z)_{(\text{sub})} = \phi_{\mathbf{g}} \exp\left(2\pi i s z - \frac{\pi i z}{\xi_{\mathbf{0}}} + 2\pi i \mathbf{g}.\mathbf{R}\right) \qquad (26.3)$$

The justification for this substitution is the same as always. You'll notice that $\phi_{\mathbf{0}}(z)_{(\text{sub})}$ is the same as before, but $\phi_{\mathbf{g}_{(\text{sub})}}$ now includes a **g**.**R** term. The reason for this substitution is that it will give us a simple expression for $d\phi_{\mathbf{g}}/dz$.

The equations become

$$\frac{d\phi_{\mathbf{0}}(z)_{(\text{sub})}}{dz} = \frac{\pi i}{\xi_{\mathbf{g}}}\phi_{\mathbf{g}}(z)_{(\text{sub})} \qquad (26.4)$$

and

$$\frac{d\phi_{\mathbf{g}(\text{sub})}}{dz} = \frac{\pi i}{\xi_{\mathbf{g}}}\phi_{\mathbf{0}}(z)_{(\text{sub})} + \left[2\pi i\left(s + \mathbf{g}\cdot\frac{d\mathbf{R}}{dz}\right)\right]\phi_{\mathbf{g}}(z)_{(\text{sub})} \qquad (26.5)$$

which can be rewritten, while dropping the subscript

$$\frac{d\phi_{\mathbf{g}}}{dz} = \frac{\pi i}{\xi_{\mathbf{g}}}\phi_{\mathbf{0}} + 2\pi i s_{\mathbf{R}}\phi_{\mathbf{g}} \qquad (26.6)$$

This equation looks just like equation 13.14 but with $s_{\mathbf{R}}$ instead of s, where

$$s_{\mathbf{R}} = s + \mathbf{g}\cdot\frac{d\mathbf{R}}{dz} \qquad (26.7)$$

The concept of $s_{\mathbf{R}}$ is new.

The importance of this result is that although we have a new 's.' we have the same equation so we can use the rest of the analysis of Chapter 13 and obtain the same results with a modified value of s, i.e., $s_{\mathbf{R}}$. Therefore, we'll have the same thickness dependence so that the contrast of the defects will depend on both **s** and $\xi_{\mathbf{g}}$. The big change is that we can now treat the case where **R** is a continuous function of z.

We will examine how the $\mathbf{g}.d\mathbf{R}/dz$ and **g**.**R** terms are used to understand dislocations. Since the equations we have just derived have the same form as those we discussed in Chapters 13 and 25, we can expect many of the same properties in the images. In particular, the images of defects will show the same sort of thickness dependence. We can also use the equations we derived in Chapter 25, so we have two ways of looking at the defects

- **g**.**R** contrast is used when **R** has a single value,
- $s_{\mathbf{R}}$ contrast is used when **R** is a continuously varying function of z, which in turn is associated with $\mathbf{g}.d\mathbf{R}/dz$.

Now let's consider the principles of this analysis. Remember, we are not trying to be quantitative or totally rigorous. We will generalize the two-beam treatment for the imperfect crystal. Note that we still have beams, it's a dynamical situation, and we assume that the column approximation is valid. So how does the column approximation relate to the theory? The model relates **R** to the column as shown in Figure 26.3 and the calculation is for a continuum even though we have atoms. The important point is that the displacement field, **R**, varies with position, **r**; we can define the origin as the core of the defect. We'll go through the calculation for a dislocation parallel to the foil surface.

As we saw in Section 13.11, the column approximation is equivalent to assuming that the crystal can be divided into narrow columns. We then calculate the amplitudes of the beams in any such column as if the whole crystal consisted of an infinite number of identical columns. The approximation is valid when we don't need to see image detail below 2–3 nm. The actual diameter of the column depends on the diffracting conditions. We can include the effect of distortions due to strains from lattice defects by imagining that the column consists of slabs of perfect crystal, each displaced by an amount $\mathbf{R}(z)$ (like a mini-SF that's different on every plane). Remember that z is actually measured along the column.

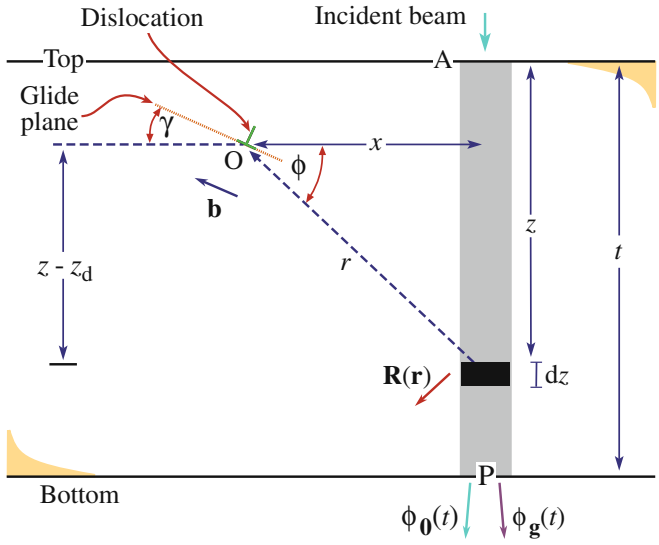

FIGURE 26.3. The effect of a dislocation with Burgers vector, **b**, at O on a column, distance x away. The effect of the strain field on the electron waves in the column is integrated in increments dz over its total length t, giving amplitude $\phi_{\mathbf{0}}(t)$ and $\phi_{\mathbf{g}}(t)$ at P.

26.3 CONTRAST FROM A SINGLE DISLOCATION

When we study dislocations, we usually want to know how many there are (the density) and whether they are edge, screw, or mixed in character. The displacement field in an isotropic solid for the general, or mixed, case can be written as

$$\mathbf{R}=\frac{1}{2\pi}\left(\mathbf{b}\phi+\frac{1}{4(1-\nu)}\{\mathbf{b}_e+\mathbf{b}\times\mathbf{u}(2(1-2\nu)\ln r+\cos 2\phi)\}\right) \tag{26.8}$$

For convenience, **R** is given here in polar coordinates (r and ϕ) shown in Figure 26.3; **b** is the Burgers vector, $\mathbf{b}_e$ is the edge component of the Burgers vector, **u** is a unit vector along the dislocation line (the line direction), and ν is Poisson's ratio.

It was particularly important to be able to write down this expression when we did the calculations by hand. However, when we have a computer available, it's quite straightforward to use anisotropic elasticity or just feed in displacements calculated from a computer model of the atom structure.

The amplitude of the diffracted beam, $\phi_{\mathbf{g}}$, is directly influenced by the value of **R**. We can consider two particular cases, namely, the screw and edge dislocations. For the screw dislocation, $\mathbf{b}_e = 0$ and **b** is parallel to **u** so that $\mathbf{b}\times\mathbf{u} = 0$. Then the expression for **R** in equation 26.8 simplifies to

$$\mathbf{R} = \mathbf{b}\frac{\phi}{2\pi} = \frac{\mathbf{b}}{2\pi}\tan^{-1}\left(\frac{z-z_d}{x}\right) \tag{26.9}$$

Here, z is the distance traveled down the column and z_d is the distance of the dislocation core below the top surface (again, refer to Figure 26.3). The dependence on $(z - z_d)$ emphasizes that the displacement field is present above and below the dislocation; it affects the whole column. From these two equations we see that **g**.**R** is proportional to **g**.**b**. For this reason, we often discuss images of dislocations in terms of **g**.**b** (g-dot-b) contrast. Examples of **g**.**b** values for some dislocations lying on a (111) plane in an fcc material with a [011] beam direction are given in Table 26.1.

TABLE 26.1. Different Burgers Vectors and Different Reflections Give Different g.b = *n* Values

g \ b	$\frac{1}{6}[11\bar{2}]$	$\frac{1}{6}[1\bar{2}1]$	$\frac{1}{6}[\bar{2}11]$	$\frac{1}{3}[111]$
$\pm(1\bar{1}1)$	$\pm\frac{1}{3}$	$\pm\frac{2}{3}$	$\pm\frac{1}{3}$	$\pm\frac{1}{3}$
$(\bar{1}\bar{1}1)$	$\pm\frac{2}{3}$	$\pm\frac{1}{3}$	$\pm\frac{1}{3}$	$\pm\frac{1}{3}$
$(0\bar{2}2)$	± 1	± 1	0	0
(200)	$\pm\frac{1}{3}$	$\pm\frac{1}{3}$	$\pm\frac{2}{3}$	$\pm\frac{2}{3}$
$(3\bar{1}1)$	0	± 1	± 1	± 1
$(\bar{3}\bar{1}1)$	± 1	0	± 1	± 1

The dislocations all lie on a (111) plane in an fcc material; the beam direction is [011].

THE SPECIMEN

If the sample is a single crystal, then you need to prepare a specimen with a [111] foil normal, so that you can image long segments of the dislocations lying in the plane of the foil on their (111) glide plane.

The second special case arises when the dislocation is pure edge in character. Then $\mathbf{b} = \mathbf{b}_e$ and **g**.**R** involves two terms **g**.**b** and **g**.**b** × **u**. (The latter term is read as 'g-dot-b-cross-u.') The displacement field causes the Bragg-diffracting planes associated with **g** to bend. Incidentally, the origin of **g**.**b** × **u** is interesting; it arises because the glide plane is buckled by the presence of an edge dislocation as illustrated in Figure 26.4. This buckling can be important because it complicates the analysis of **b** for some dislocations with an edge component, as we'll see below.

- Always remember: **g**.**R** causes the contrast and for a dislocation, **R** changes with z.
- We say that **g**.**b** = n. If we know **g** and we determine n, then we know **b**.

An experimental point: you usually set s to be greater than 0 for **g** when imaging a dislocation in two-beam conditions. Then the dislocation can appear dark against a bright background in a BF image. Of course, you still need to think about $s_{\mathbf{R}}$ and $d\mathbf{R}/dz$ since these will vary with z, as we saw in Figure 26.1.

The + and – signs in Table 26.1 are very important. If the sign of **R**, and hence **g**.**R** or **g**.**b**, reverses, then the image of the dislocation will move to the other side of the projected

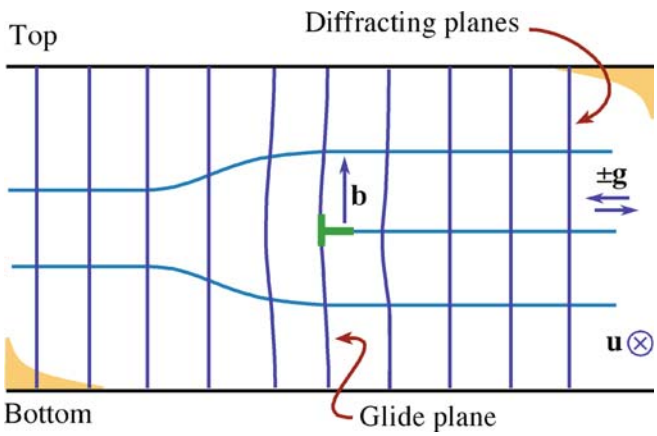

FIGURE 26.4. Buckling of the glide planes arises because of the term **g**.**b** × **u** and is important because it complicates the analysis of **b**.

position of the dislocation core. If you look carefully at Figure 26.1, you can appreciate that reversing the sign of s produces the same effect as reversing the sign of **g**. We can summarize these two ideas in terms of the quantity (**g**.**b**)s ('g-dot-b-times-s'), as shown in Figure 26.5.

If we identify two reflections $\mathbf{g}_1$ and $\mathbf{g}_2$ for which $\mathbf{g}.\mathbf{b} = 0$, then $\mathbf{g}_1 \times \mathbf{g}_2$ is parallel to **b**. This identification of **b** is actually a little more complicated because dislocations appear out of contrast when $\mathbf{g}.\mathbf{b} < 1/3$; similarly, dislocations need not be invisible even if $\mathbf{g}.\mathbf{b} = 0$ when $\mathbf{g}.\mathbf{b} \times \mathbf{u} \neq 0$.

INVISIBILITY CRITERION
If $\mathbf{g}.\mathbf{b} = 0$, then you won't see any contrast because the diffracting planes are then parallel to **R**.

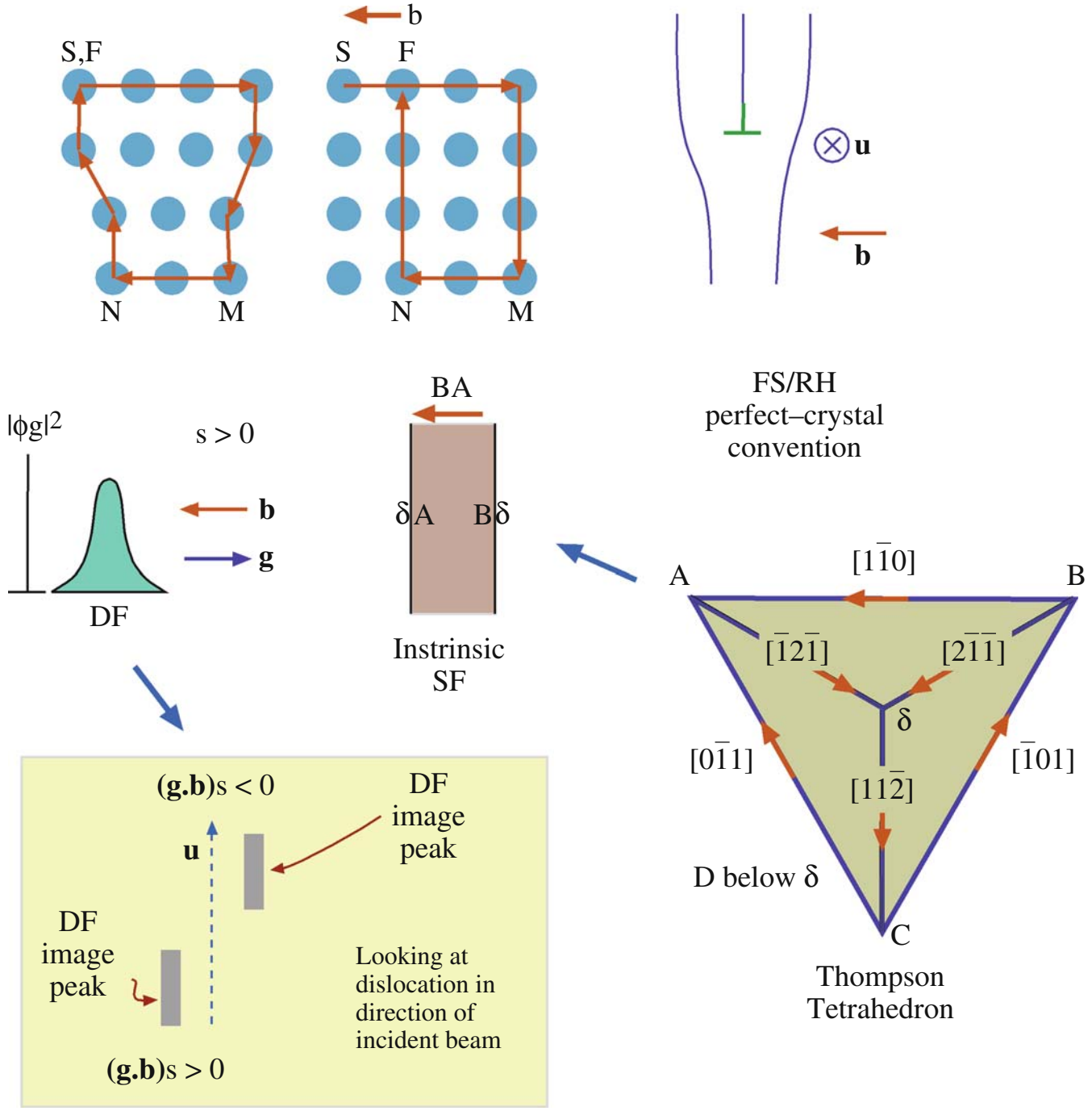

FIGURE 26.5. A brief summary of dislocations in an fcc crystal: **b** is defined by the finish- (F) to-start (S) vector in a right-hand (RH) circuit that comes to closure around the dislocation but fails to close in the perfect crystal. The location of the diffracted intensity $|\phi_{\mathbf{g}}|^2$ relative to the core depends on the sign of **b**, **g**, and s for the FSRH convention. If any sign is reversed, the contrast shifts across the core. When a perfect dislocation splits into Shockley partial dislocations, the order of the partial dislocation is given by the Thompson tetrahedron.

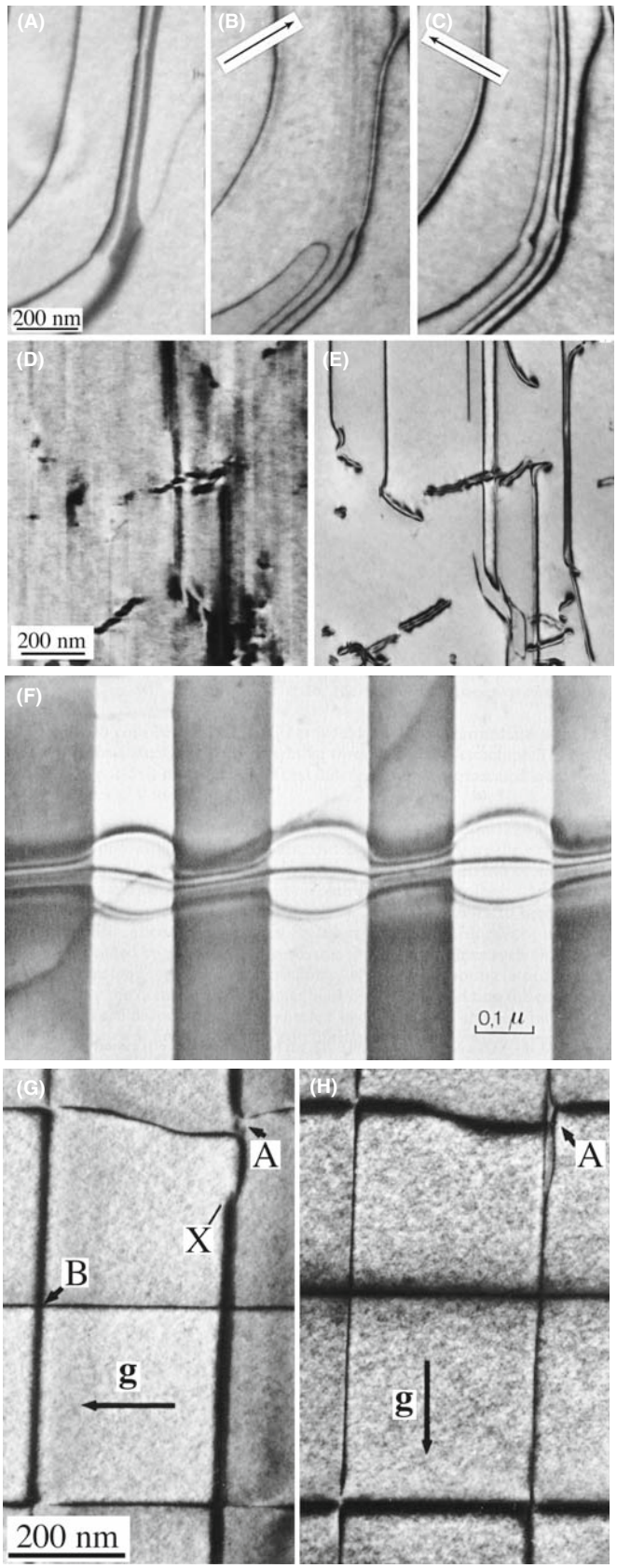

If we compare the contrast from a dislocation with that from a SF, the difference is that now α is a continuously varying function of z. The image of the dislocation itself shows thickness fringes but it may be 'out of contrast' at some depths or thicknesses, as you can see (look carefully) in the experimental image shown in Figure 26.6E.

Some points to remember from this discussion are

- The sign of s affects the image.
- The sign of x affects the image; the image is asymmetric.
- The magnitude of s affects the image.
- The depth of the dislocation and the thickness of the specimen affect the image.
- The appearance of the image depends on $\mathbf{g}.\mathbf{b}$ or, more completely, on $(\mathbf{g}.\mathbf{b})s$ and $\mathbf{g}.\mathbf{b} \times \mathbf{u}$.
- If we repeat this analysis for other values of $\mathbf{g}.\mathbf{b}$ $(= n)$ and plot intensities, we would find that the image width becomes broader as n increases.
- Note where the dislocation image 'comes from': the position of the line in the image only rarely corresponds to the projected position of the dislocation; it is usually displaced to one side of the core.
- As a complication, remember that the dislocations will probably be found in wedge specimens, not ideal parallel-sided ones.

A final 'rule of thumb' which you may find useful (from computer modeling and early analytical calculations) is that if $\mathbf{g}.\mathbf{b} = 0$, you can still 'see' dislocations when $\mathbf{g}.\mathbf{b} \times \mathbf{u} \geq 0.64$. For fcc materials, this rule can be useful when the foil is not parallel to a {111} plane.

Other examples of dislocation images are illustrated in Figure 26.6. Remember that partial dislocations are not only present in fcc metals; they also occur in many fcc semiconductors and many layer materials. Such materials may have a very low stacking-fault energy allowing the partial dislocations to separate, forming wide ribbon-like defects, as shown in Figure 26.6A–C. The single 'line' (that is actually a dark line and a less-dark line) below the arrow in (C) is a dislocation having its Burgers vector parallel to $\mathbf{g}$ (so $\mathbf{g}.\mathbf{b} = 2$); you can see two 'peaks' in the image, one darker and broader than

FIGURE 26.6. (A–C) Three strong-beam BF images from the same area using (A) $\{11\bar{1}\}$ and (B, C) {220} reflections to image dislocations which lie nearly parallel to the (111) foil surface in a Cu alloy which has a low stacking-fault energy. (D, E) Dislocations in Ni_3Al in a (001) foil imaged in two orthogonal {220} reflections. Most of the dislocations are out of contrast in (D). (F) A complex dislocation crossing a (rotational) domain boundary; the character of the dislocation changes and thus its dissociation width changes. (G, H) Dislocations of a (001) interface between two slightly lattice-mismatched III–V compounds.

the other. Notice that one of those dark lines in (C) has nearly disappeared in (B) and the dark peak is on the other side of the dislocation. A group of three parallel lines is present in (C) but is almost out of contrast in (B). These are Shockley partial dislocations all having the same **b** and thus giving **g**.**b** = 0 in (B) (the three lines actually form by the dissociation of a perfect dislocation with Burgers vector $\frac{1}{2}<112>$). The $11\bar{1}$ image (A) is formed by tilting the specimen to a 112 pole (~20° from the 111 pole) and shows contrast from the stacking faults themselves (imagine them filling the area between the dislocations); these faults will never give contrast at the 111 pole since **g**.**R** is then always 0 (or an integer). Intermetallics tend to have large unit cells so that the superlattice dislocations dissociate into partial dislocations, which would have been perfect dislocations in the disordered crystal (Figure 26.6D and E). These super-partial dislocations can dissociate further as they might have in the disordered lattice, or they can separate differently in different ordered domains (Figure 26.6F). Dislocations in interphase boundaries can be revealed by imaging with different reflections (Figure 26.6G and H). Since the dislocations are present to accommodate the mismatch, they must lie at, or close to, the (001) phase boundary. It can be difficult to analyze their Burgers vectors unambiguously, because the adjoining materials have different extinction distances, etc. The topic is 'image interpretation': now you know why. One of the extra challenges is determining the plane on which this dissociation occurs. We'll illustrate how we can see **g**.**b** × **u** contrast when we examine dislocation loops in Zn in Section 26.6.

A QUESTION

How many dislocations can you really see in Figure 26.6H? Answer: zero.

26.4 DISPLACEMENT FIELDS AND EWALD'S SPHERE

In Section 26.2, we showed that when a displacement **R**(**r**) is present, we can think of s as being replaced by $s_{\mathbf{R}}$ (equation 26.7). This new s should be written more completely as

$$s_{\mathbf{R}} = s + \mathbf{g}.\frac{\partial R}{\partial z} + \theta_B \mathbf{g}.\frac{\partial \mathbf{R}}{\partial x} \qquad (26.10)$$

The point is that, as you can see in Figure 26.7, **R** causes the lattice planes to bend through an angle δϕ. So two other parameters, namely **g** and s, also change. The diffraction vector is actually lengthened by Δ**g** but, more

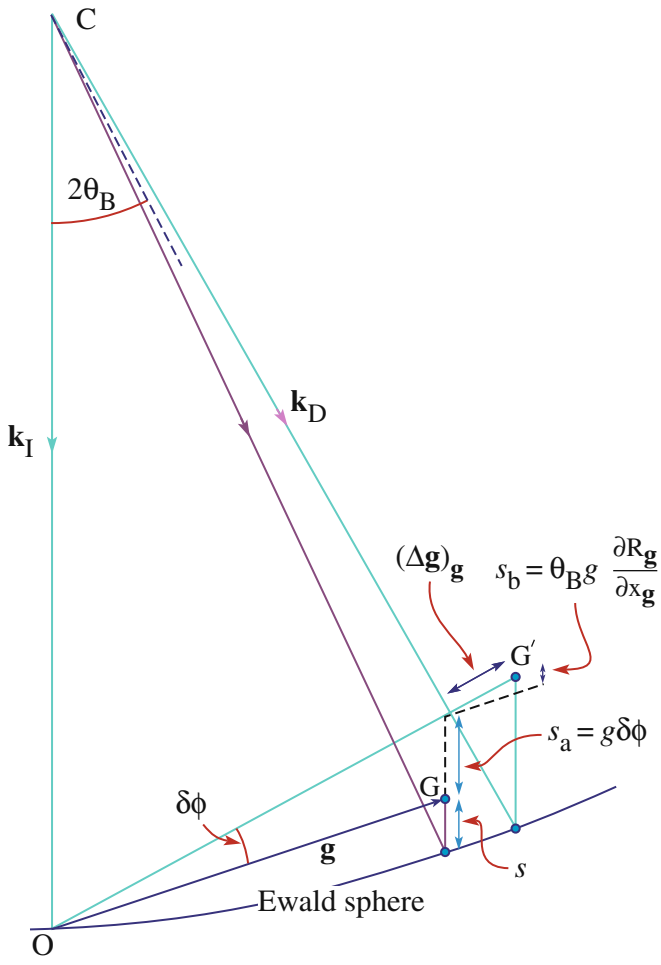

FIGURE 26.7. The strain field of the dislocation causes the lattice planes to bend through an angle δϕ. So **g** and s also change. The diffraction vector is lengthened by Δ**g** and **g** is rotated. So s increases by the two components of $s_{\mathbf{R}}$, i.e., s_a and s_b.

importantly, **g** is rotated. The result is that **s** increases by the two components s_a and s_b shown in the figure, to give $s_{\mathbf{R}}$. If you manipulate this equation for small angles you can produce equation 26.7. We usually neglect the third term because θ_B is small but it can become important when screw dislocations intersect the surface.

An alternative way of looking at this deformation is to think of **g** as changing by Δ**g**. We can define this change by the equation

$$\mathbf{g}.(\mathbf{r} - \mathbf{R}(\mathbf{r})) = (\mathbf{g} + \Delta\mathbf{g}).\mathbf{r} \qquad (26.11)$$

so that

$$-\mathbf{g}.\mathbf{R}(\mathbf{r}) = \Delta\mathbf{g}.\mathbf{r} \qquad (26.12)$$

The implication is that the information about the displacement field, **R**(**r**), is present in the region around **g** but not actually at **g**. Remember that the reflection **g** is present because we have a perfect crystal. It is difficult to image this type of scattering (but it becomes easier using

EFTEM). If you displace the objective aperture, you will still see the dislocation, but other inelastic scattering will complicate image interpretation. We saw that scattering does indeed occur between Bragg reflections in Section 17.6. An analogy for scattering from dislocations is the scattering of light from a single slit which we discussed in Chapter 2.

In the deformable-ion approximation (Section 25.13), we make the assumption that the atom doesn't know it has moved. If **R**(**r**) varies rapidly, as it does near the core of a dislocation, the approximation must fail. You can draw the same conclusion whenever the density of the material changes rapidly. So what we should do is use a better model for the atomic potential, one that also takes account of what happens to the valence electrons at such a defect. Of course, linear elasticity theory also fails when the strains, and hence **R**(**r**), are large, as at dislocation cores.

26.5 DISLOCATION NODES AND NETWORKS

You can analyze the Burgers vectors of dislocations which form networks directly and easily, if all the dislocations lie in a plane parallel to the surface of the specimen, as illustrated in Figure 26.8 for the case of graphite. The idea is simple: you form a series of images using different **g**-vectors. Don't forget that you can tilt to other poles; in fact, you'll often need to tilt the specimen just to image SFs which lie parallel to the foil surface, as in Figure 26.8A (but you won't see SF fringes then). When the diffraction vector is parallel to the plane of the SF you'll only see contrast from the dislocations as in Figure 26.8B–D. Such tilting experiments are essential if you're examining networks of misfit dislocations since the dislocations will then often have a component of their Burgers vector out of the plane of the network.

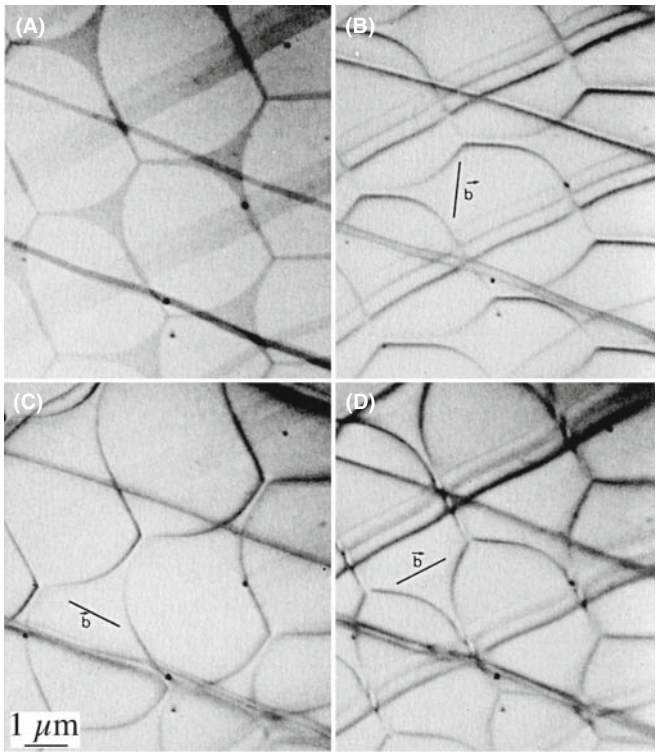

FIGURE 26.8. Dislocation networks in graphite. In (A) the stacking faults parallel to the foil surface are imaged by using a **g** that is inclined to the fault (so **g**.**R**≠ 0); in (B–D) two of the three dislocations at each node are in contrast but the third is invisible. Knowing **g** for each image, the Burgers vector of the dislocations can be determined as shown in (B–D) (**g**.**b** = 0 for the *missing* dislocations).

26.6 DISLOCATION LOOPS AND DIPOLES

Loops have been studied extensively because they can form when point defects coalesce. There are probably thousands of papers describing TEM studies of radiation damage and the formation of dislocation loops. In fact, many HVEMs were built in the 1960s just to study this problem. Questions which were answered led to a greatly improved understanding of irradiation processes (but failed to justify the construction of more nuclear power stations). We found that

- The loops can form by coalescence of interstitials or vacancies.
- The rate of growth, critical size, and nucleation time for different loops can be measured.
- Some of the loops are found to be faulted (containing a SF) while others are not faulted. The faulting should be related to the size of the loop and the stacking-fault energy of the material.

These studies were particularly instructive illustrations of the value of diffraction contrast.

- Dislocation loops can have either positive or negative **b,** and can be inclined to the beam on different planes as shown in Figure 26.9. Many person-years have been spent analyzing the inside-outside contrast from such defects to determine if they were caused by vacancies or interstitials.
- Loops can be present that show no **g**.**b** contrast.
- Loops can enclose single or multiple stacking faults, and so exhibit SF contrast as shown in Figure 26.10.
- The dislocation dipole is a special case and gives an important example of interacting dislocations. TEM is the best way to image dipoles because they have no long-range strain fields; the Burgers vector of the complete dipole is zero! (More on this in Chapter 27.)

Dislocations in Zn provide a particularly nice illustration of **g**.**b** × **u** contrast. If the specimen surface is parallel

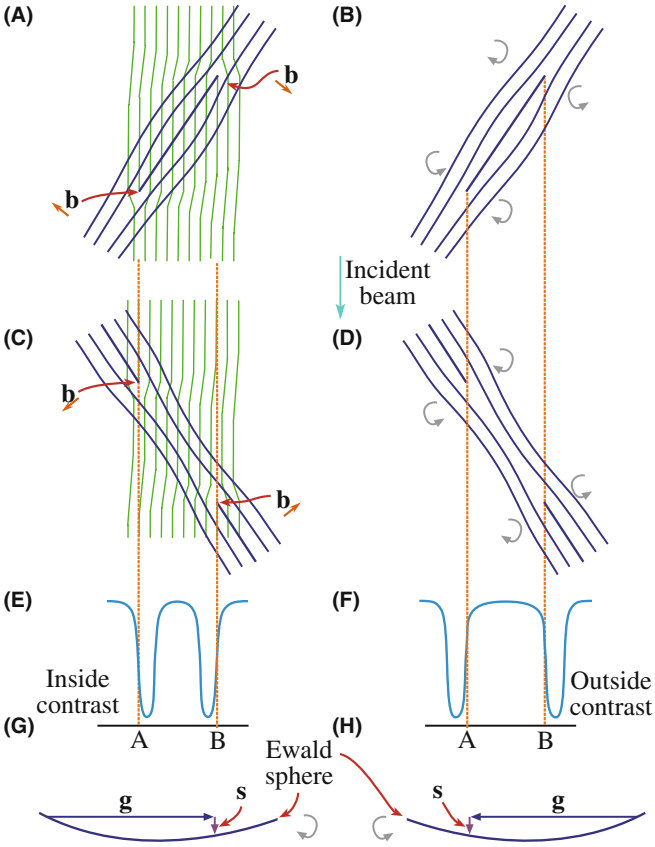

FIGURE 26.9. (A) Structure of an interstitial loop relative to the diffracting plane (faint lines). (B) Arrows show the rotation of the diffracting planes around the dislocation. (C, D) Vacancy loops. (E, F) Position of the image contrast relative to the projected dislocation position. Inside contrast occurs when clockwise rotation of the diffracting planes brings them into the Bragg condition. Outside contrast occurs for the counterclockwise case. (G, H) The relationship between **g**, **s**, and the sense of rotation. Everything is reversed if the loops are tilted in the opposite direction relative to the beam (i.e., reflect this figure in a mirror).

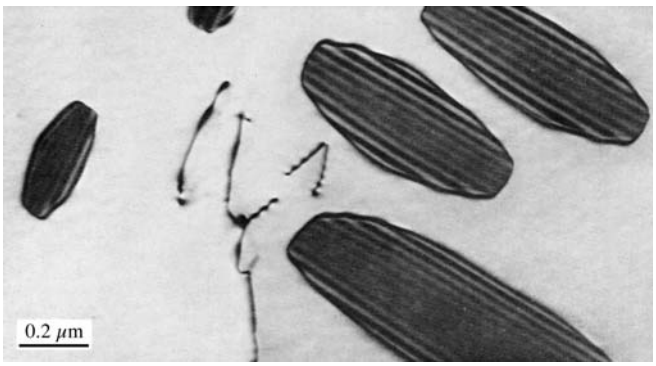

FIGURE 26.10. Dislocation loops in irradiated Ni showing SF contrast.

to the (0001) basal plane, then dislocation loops can readily form by coalescence of vacancies. In Figure 26.11, **b** is normal to **g** so that **g**.**b** = 0. These loops give a clear illustration of how the appearance of the image

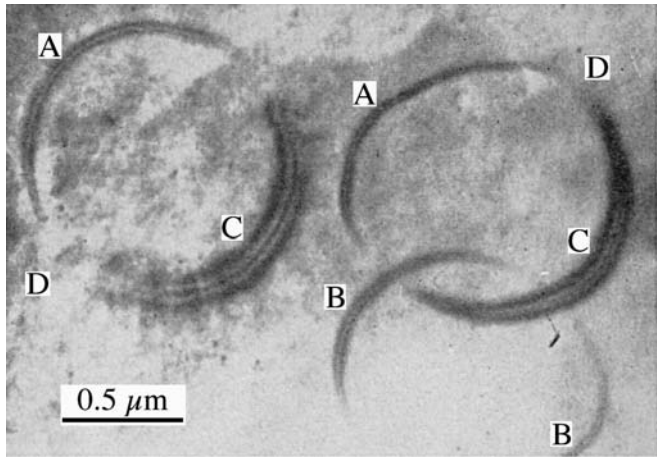

FIGURE 26.11. Prismatic loops in Zn parallel to the (0001) surface of the specimen with **b** = *c*[0001]. All round the loop, **b** is normal to **g** so that **g**.**b** = 0 and the vector **b** × **u** lies in the plane of the loop. At A, B, and C, **b** × **u** is parallel to **g** so that we see strong contrast. However, at D, **b** × **u** and **g** are mutually perpendicular so that **g**.**b** × **u** = 0 and the loop disappears.

depends on the line direction, **u**, of a dislocation. Note that you can see the dislocation contrast, even though **g**.**b** is zero, so this is not an absolute criterion for invisibility.

The above discussion is fine if the loops are large, but a problem arises when they are small. You must then consider the details of the contrast mechanism.

This was, of course, true for all these images, but now the size of the defect is small compared to the extinction distance. The schematic shown in Figure 26.12 summarizes the contrast that arises from small vacancy loops; if the loops were interstitial in nature, the contrast would be reversed. Not only does the black/white contrast change as the position of the defect changes in the specimen, but its size also appears to change. When the nature of the loops becomes more complex, the appearance of the image may also become more difficult to interpret with 'butterflies,' 'lozenges,' and 'peanuts' being seen. Notice that the behavior of the contrast differs in the BF and DF images; this effect is similar to that which we discussed in Chapter 25 and is again related to anomalous absorption.

IMAGES AND THICKNESS

The basic idea is that the appearance of the image is now dependent on the thickness of the specimen.

Dislocation dipoles can be present in great numbers in heavily deformed metals, but can also be important in the degradation of some semiconductor devices. Dipoles can be thought of as loops which are so elongated that they look like a pair of single dislocations of opposite Burgers vector, lying on parallel glide planes. As a result, they are best recognized by their

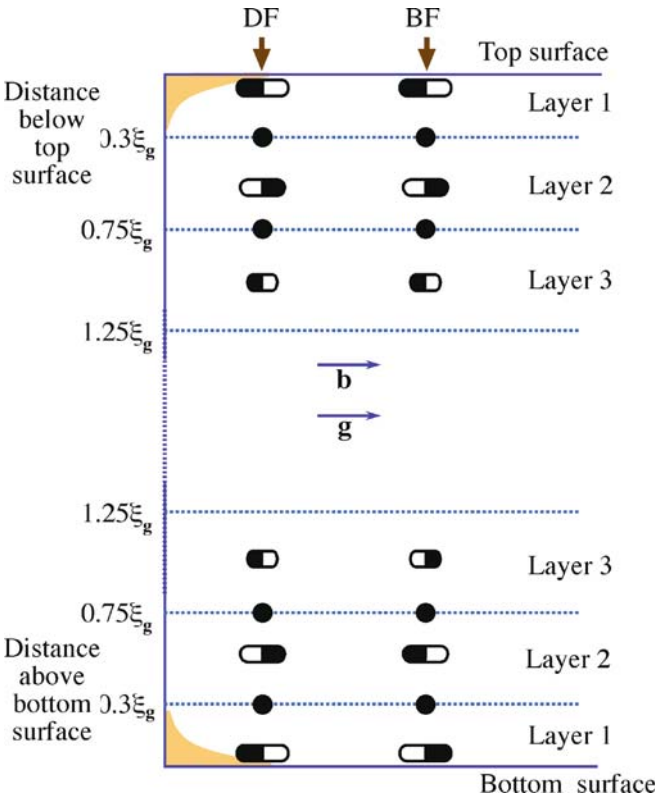

FIGURE 26.12. Changes in the black-white contrast from small dislocation loops at different depths in the specimen. The DF shows the same contrast at top and bottom while the BF contrast is complementary at the two surfaces.

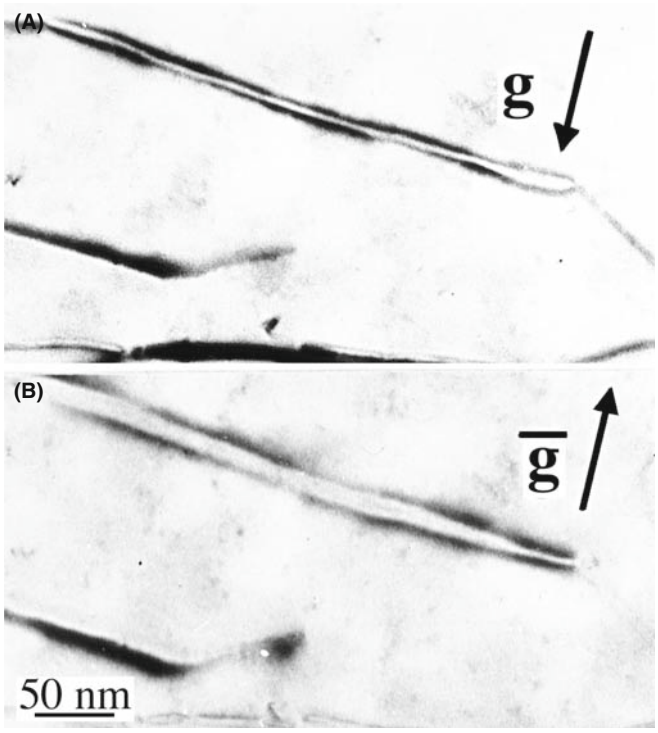

FIGURE 26.13. Images of dislocation dipoles in Cu showing inside-outside contrast on reversing **g** (±220). (A) is inside; (B) is outside.

'inside-outside' contrast, as illustrated in Figure 26.13. You can appreciate the origin of the term by looking at the projection of the images of the two dislocations when you reverse the sign of **g**: since the two dislocations have opposite Burgers vectors, Figure 26.9 tells you that one image will lie on one side of the core and the other on the opposite side. The order reverses when we reverse **g**.

26.7 DISLOCATION PAIRS, ARRAYS, AND TANGLES

Remember, you are not limited to **g**-vectors which are parallel to the foil surface; hence you can tilt the specimen to see SF contrast. As we saw in Figure 26.8A, this is often helpful if you have SFs associated with the dislocations; you can then produce **g**.**R** contrast for the fault. We will discuss dislocation dissociation more in Chapter 27. If you look back at Figure 26.6 or 26.8, you will see the benefit of being able to see the SF. This figure also illustrates the effect of n on the dislocation contrast.

Consider a dislocation in an fcc metal which can dissociate into two Shockley partial dislocations on the (111) plane. We can write down the dislocation reaction as

$$\tfrac{1}{2}[1\bar{1}0] = \tfrac{1}{6}[1\bar{2}1] + \tfrac{1}{6}[21\bar{1}] \text{ on } (111) \qquad (26.13)$$

If we image this dislocation using the $(2\bar{2}0)$ reflection, then $\mathbf{g}.\mathbf{b} = 2$. If, instead, we use the $(20\bar{2})$ reflection, then $\mathbf{g}.\mathbf{b} = 1$. The appearance of the image is very different even if we cannot see the individual partial dislocations.

The advantage of using high voltages to study arrays of dislocations is illustrated in Figure 26.14; everything we said in Chapter 11 applies when we study dislocations. We see thickness fringes at the surface, but these disappear in the central region of the foil—the contrast becomes constant. When the foils are this thick, you may find stereomicroscopy helpful in giving a 3D view of the defect arrangement; you can imagine its value in interpreting an image such as that shown in Figure 26.15A. The defects may be very close together in heavily deformed materials, as shown in Figure 26.15B; of course, the interpretation of such an image depends on the thickness of the specimen so you also need to know the voltage used to form the image. Ideally, make the specimen thin over very large areas to minimize image overlap. If the density of defects is too large, the weak-beam technique may be the only way to 'look into' the walls (Chapter 27) but then the specimen needs to be even thinner.

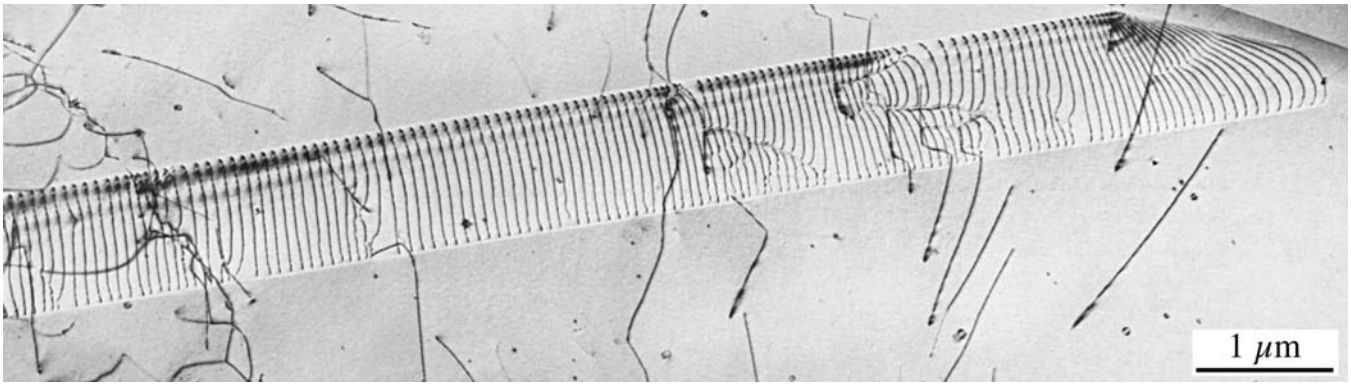

FIGURE 26.14. Dislocations threading through a very thick specimen in an image recorded using a (very) high-voltage (3 MeV) TEM.

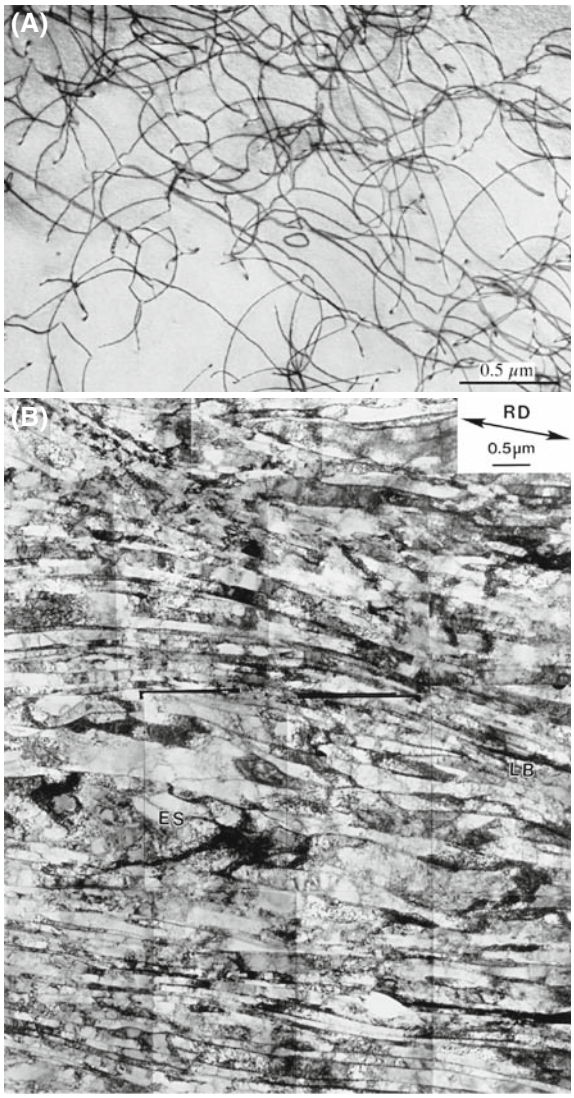

FIGURE 26.15. (A) Dislocation tangles in an Fe-35% Ni-20% Cr alloy, creep tested at 700°C; the dislocations have moved by glide and climb and do not lie on well-defined planes. (B) Dislocation walls in Al which has been heavily deformed by directional rolling. (200-keV electrons but super specimen.)

A CALCULATION

$\sin\theta_D/2 = \mathbf{b}/2t$.

If $\mathbf{b} \sim 0.25$ nm and $t = 50$ nm $\sin\theta_D/2 = 0.0025$ and $\theta_D = 0.29°$; compare to a Bragg angle from $\sin\theta_B = (n\lambda/2d)$ (0.0037 nm/0.05 nm=0.0074). θ_B=0.42°. Notice how θ_D increases for thinner foils and θ_B (and λ) decreases as voltage increases.

26.8 SURFACE EFFECTS

In TEM, we always have thin foils. Dislocation strain fields are long range, but we often assign them a cut-off radius of ~50 nm. However, the thickness of the specimen might only be 50 nm or less, so we can expect the surface to affect the strain field of the dislocation, and vice versa.

When an edge dislocation lies parallel to the surface of a very thin specimen, it causes the specimen to bend. The effect is not large, but large enough compared to the Bragg angle, as illustrated schematically and with an example in Figure 26.16.

Similarly, if the dislocation is dissociated, the proximity of the surface causes its width to decrease (as in Figure 26.16C). We can model this situation using 'image dislocations' as shown in Figure 26.16D. The main point is that we can think of these image dislocations as forcing the partial dislocations closer together; the proximity of the surface can really change the structure of the defect, not just its contrast. A similar effect can occur when the dislocation is inclined to the surface and can result in a V-shaped dissociated dislocations, as we'll show in Section 27.8.

A special interaction between dislocations and surfaces occurs when a dislocation tries to glide out of the material but can't penetrate a surface layer (which might even be amorphous, as in the case of oxide films on metals), as shown in Figure 26.17.

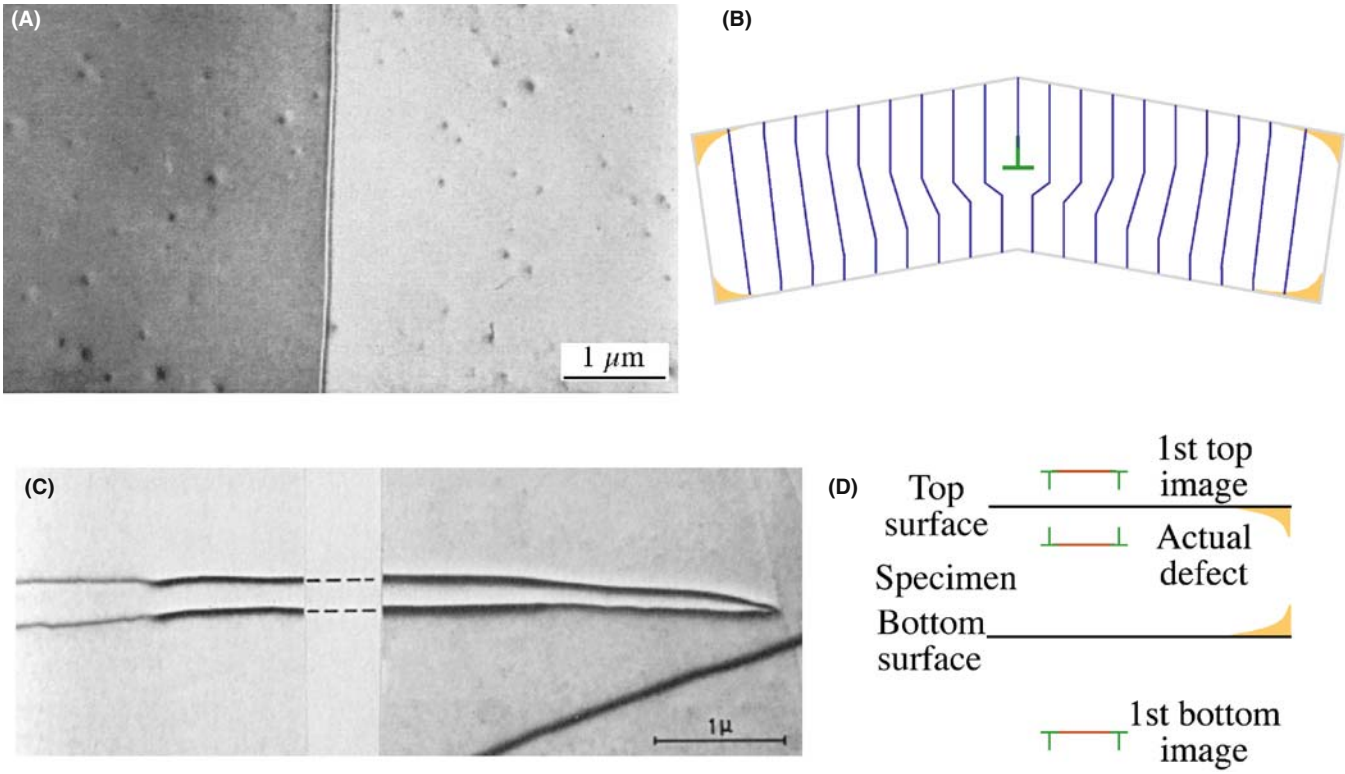

FIGURE 26.16. (A) BF image of a single-edge dislocation lying parallel to the surface of a very thin foil of SnSe, causes the diffracting planes to bend as shown schematically in (B) so we see different contrast intensity in the matrix on either side of the defect. (C, D) If the dislocation is dissociated, the image forces due to the surface cause its width to decrease as it approaches the surface. The schematic in (D) shows two image dislocations included to represent the effect of the nearest surface.

We can have dislocations at the surface just because the structure of the surface layer is different from that of the bulk material. The surface of materials can actually reconstruct. The surface of a very clean (111) Au film is actually more dense than the rest of the film and this misfit is accommodated by surface dislocations, as shown in Figure 26.18. We see the contrast because the strain field extends into the bulk layer. The identification of these dislocations has been confirmed using STM, which also gives more information on the detailed surface structure. However, they were observed first by TEM. The difficulty in TEM studies is that the surface contaminates unless you operate under UHV conditions. The same comment is true for STM of metals but we are used to having a poorer vacuum in TEM and faster/easier specimen exchanges.

GOLD

The dislocation in Figure 26.18 is one atomic plane below the surface but **g**.**b** still works.

Dislocations can be viewed nearly parallel to their line directions, when we still see contrast even for screw dislocations, as you can see in Figure 26.19A. Initially, this contrast is surprising since **g**.**b** and **g**.**b** × **u** must be zero for any dislocation. However, the screw dislocation can relax at the surface, as shown in Figure 26.19B; it gives a twist. You see the screw dislocation even though **g**.**b** = 0 because of this twist.

26.9 DISLOCATIONS AND INTERFACES

Interfaces are, of course, important in all polycrystalline materials. In metals, semiconductors, and thin films on substrates, the interaction between dislocations and interfaces is critical. So now we'll briefly examine the special features we see when combining line and planar defects, as illustrated in Figure 26.20. This is one topic where image simulation, which we'll discuss in Section 26.12, is invaluable. The location of the GB is known because we can see (just) the thickness fringes and the GB dislocations. Notice that there are also 'extrinsic' (lattice) dislocations running into the GB. This is a great figure for student questions!

When we have an array of dislocations, the strain fields overlap so that the value of **R**(**r**) for each dislocation tends to be reduced. This is the GB model of an interface.

Dislocations can be present at interfaces where the composition, or structure, or both change

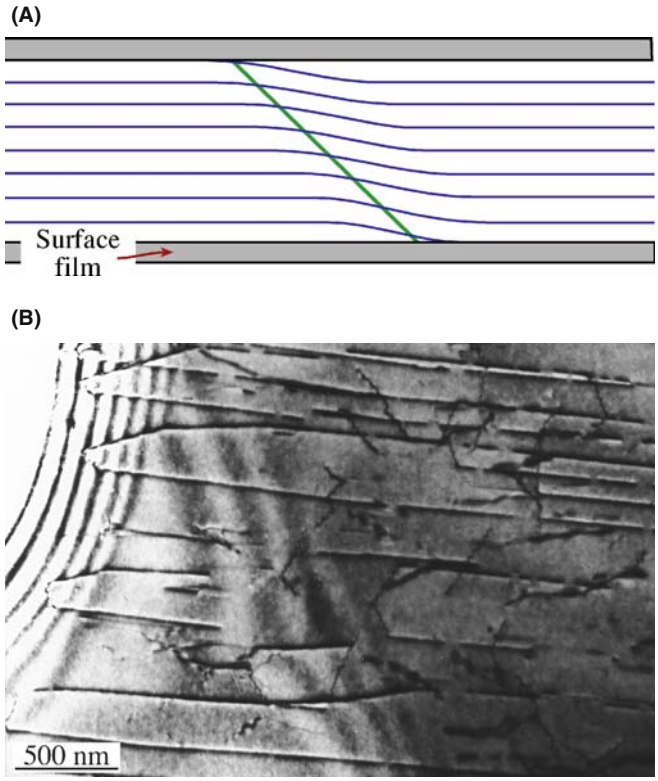

FIGURE 26.17. (A) Schematic diagram of dislocations pinned at the surface of the specimen by surface films such as oxides. (B) A reduced (i.e., metal) film on NiO pins dislocations. Such films may be introduced during or after thinning to electron transparency.

- Misfit dislocations accommodate the difference in lattice parameter between two well-aligned crystalline grains. Surface dislocations (as we saw in Section 26.8) are a special subgroup of misfit dislocations.
- Transformation dislocations are the dislocations that move to create a change in orientation or phase. The $\frac{1}{6}<112>$ dislocations in twin boundaries in fcc materials are an example of transformation dislocations (twinning dislocations).

A complication in the analysis of images of interfacial dislocations is that they are often associated with steps in the interface. There are many examples of such steps in Figure 26.21, including an example of 'step bunching.' (Notice also that **s** is different for the two grains!) Sometimes, as is the case for the $\frac{1}{6}<112>$ twinning dislocations, the dislocations must introduce a step. In other situations, steps are present but there is no dislocation. The difficulty is that we often encounter all three of these situations at the same time. We will also examine these defects using weak-beam conditions in Chapter 27 and using HRTEM in Chapter 28.

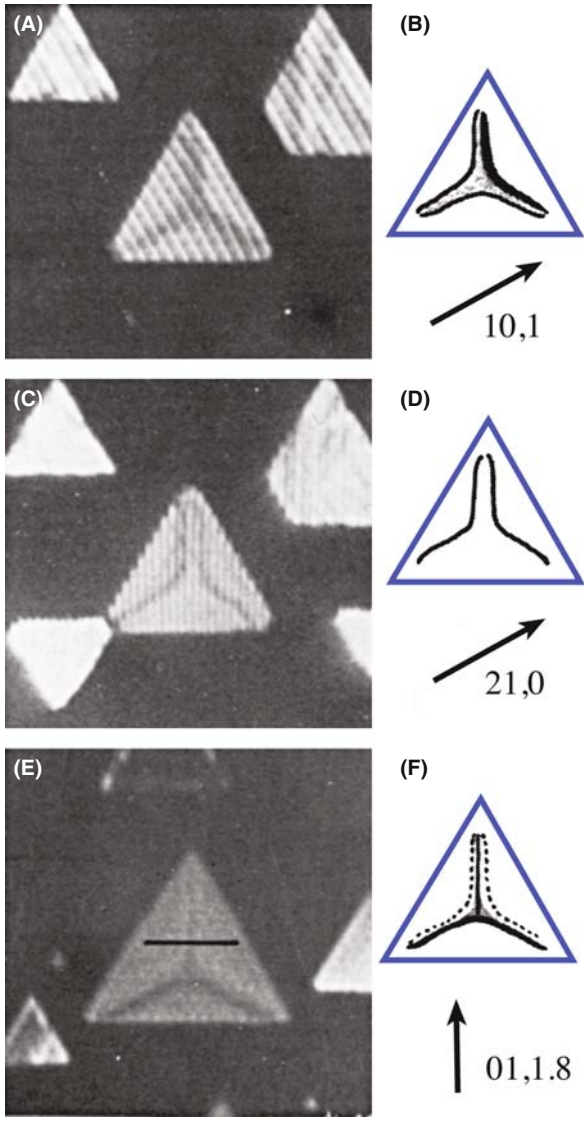

FIGURE 26.18. Dislocation networks can form at the surface of (111) Au islands because the surface layer relaxes to a 'lattice' parameter that is different from that of the bulk material. Different dislocations are visible under different diffracting conditions. The edge misfit dislocations form nodes in the triangular islands and show the usual **g**.**b** contrast behavior. (A), (C), and (E) are experimental images; (B), (D), and (F) are schematics showing **g** and summarizing the contrast.

We will discuss the images first and then, remembering that information must also be present in the DP, we will relate the two.

In many cases that interest us, GBs appear as arrays of dislocations. In general, the grains are misoriented. There are some special cases as we saw in Chapter 24.

- Two grains may have a near-common plane and therefore a nearly common, but different, **g**-vector.
- In small-angle GBs, θ is small, so the separation of the dislocations is large ($\sin\theta/2 = \mathbf{b}/2d$).

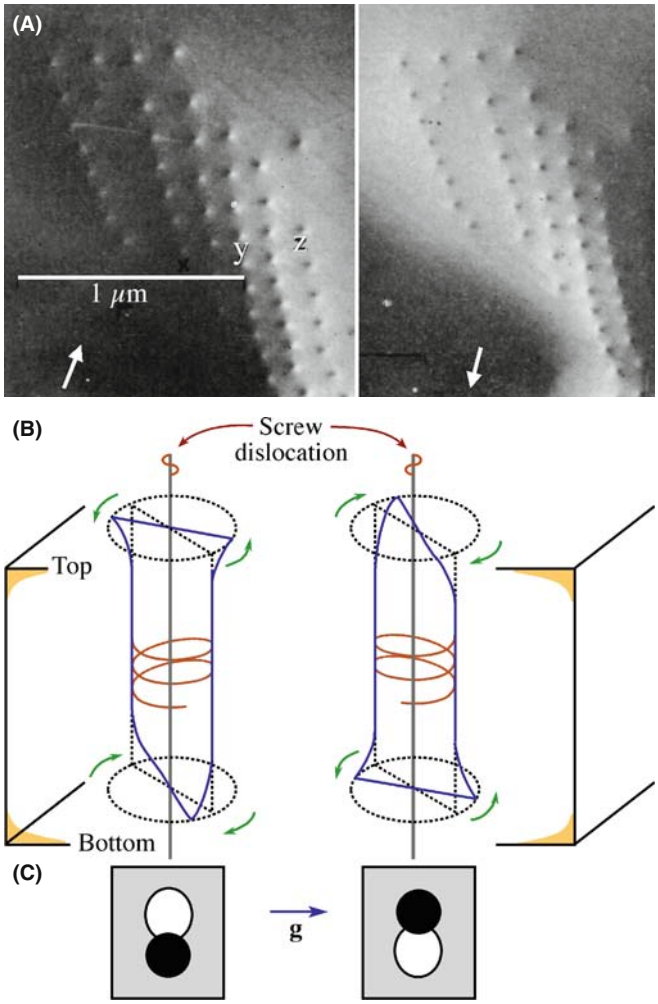

FIGURE 26.19. Screw dislocations viewed end on $\pm\mathbf{g}$. (A) Two images in $\pm\mathbf{g}$. (B) The twist relaxation at the surface. (C) Representations of the resulting contrast. The schematics in (B) show the diffracting planes rotating in the same direction away from the edge-on orientation at both surfaces.

The $\Sigma = 3$ twin boundary in fcc materials is an example of an interface where you can use common, but different, **g** vectors. Here, e.g., the $(3\bar{3}\bar{3})$ plane in one grain is parallel to the $(\bar{5}11)$ plane in the other grain (because these two reflections superimpose), and the lengths of these two **g** vectors are identical, as you can see in Figure 26.22. However, this common reflection would not normally be used to form an image because **g** is rather large. This type of coincidence of dissimilar planes can also occur for other GBs.

In the case of small-angle boundaries, we can pretend that the reflection is common to both grains. The image of the twist GB in Figure 26.23 was formed using such a 'reflection' (i.e., two nearby reflections). (Look back at Figure 17.7 to get an idea of what the DP would be like.) What we are really doing is treating the dislocations as if they were isolated lattice defects; actually, the **g** vectors for the two grains will be rotated relative to one another.

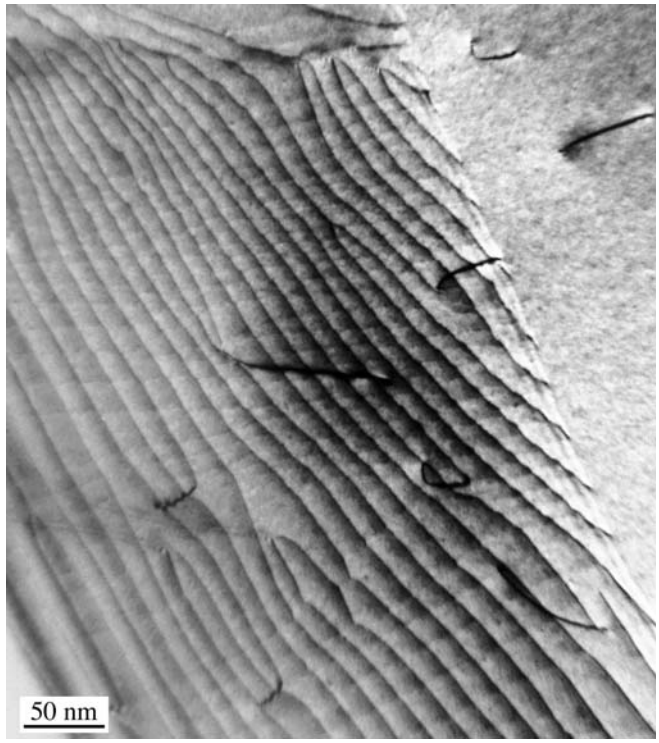

FIGURE 26.20. Dislocations interacting with a GB; the dislocation contrast changes because its strain field changes when it enters the boundary and becomes part of the dislocation structure.

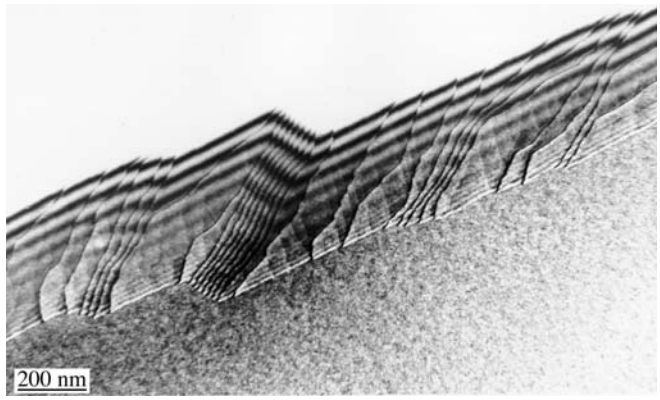

FIGURE 26.21. Steps at interfaces may also cause diffraction contrast when associated with strain. In this Ge specimen, the steps displace the thickness fringes in the GB so they are readily visible. The fringe spacing is different at the top and bottom of the boundary because the diffraction conditions are different at each grain.

Lattice misfit is very important whenever we are studying thin films; dislocations are often present to accommodate misfit. An example is shown in Figure 26.24, where dislocations are present between spinel and NiO; these two materials each have an fcc crystal structure. Although you can easily appreciate the change in lattice parameter, there is also a less obvious change in the elastic constants.

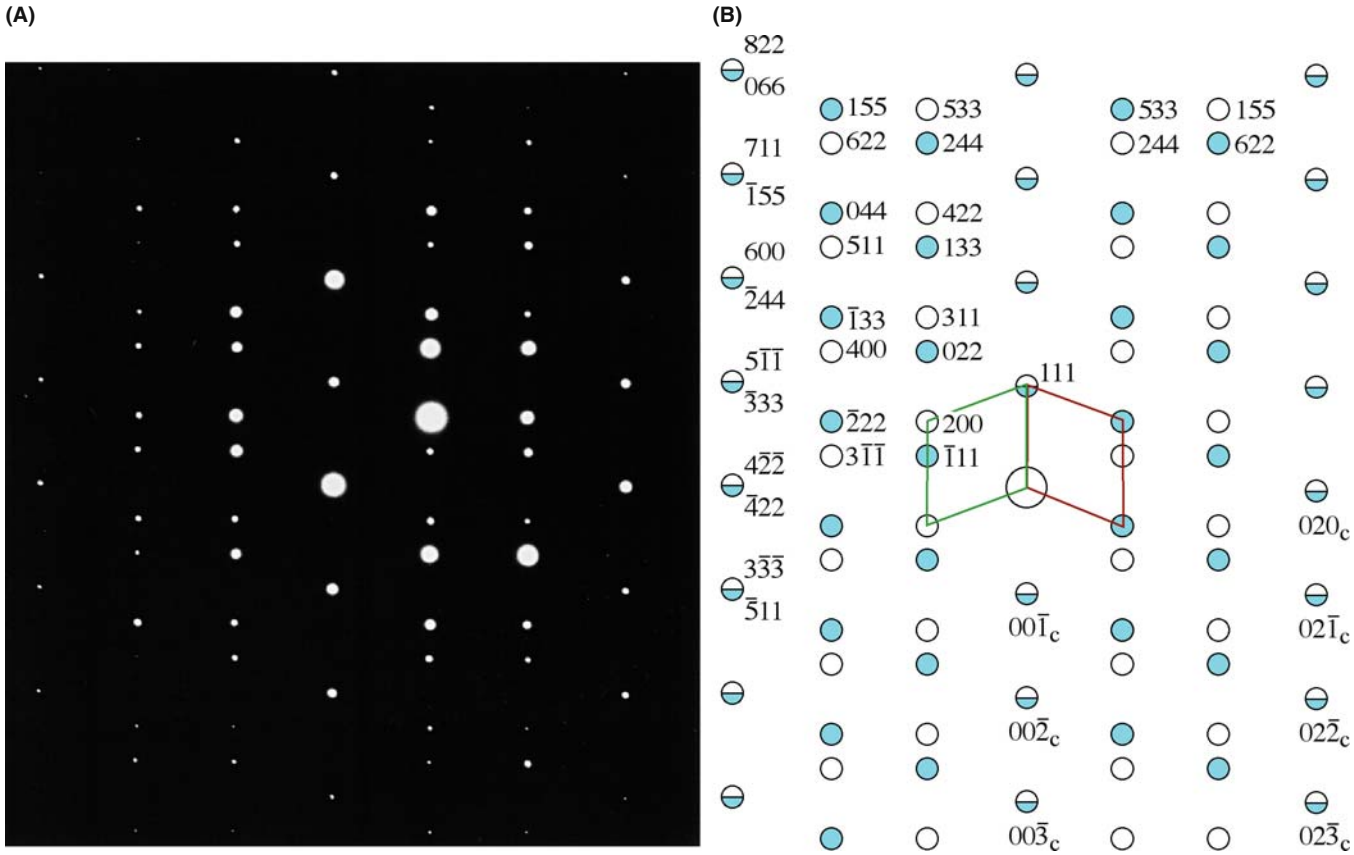

FIGURE 26.22. (A) DP and (B) its indexed schematic for a $\Sigma = 3$ twin boundary in an fcc material. Notice that many pairs of **g**-vectors exactly overlap but have very different indices.

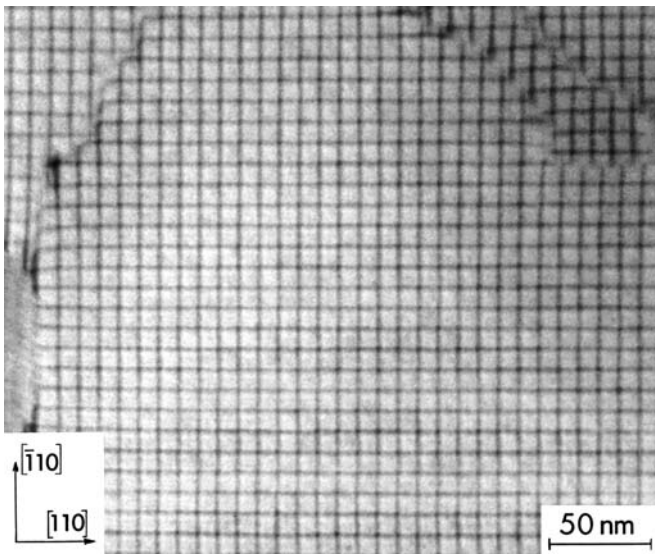

FIGURE 26.23. A low-angle (001) twist boundary in Si oriented almost exactly parallel to the specimen surface. Two (040) reflections were excited to form this BF image, but for small misorientations these are so close that we treat them as one reflection.

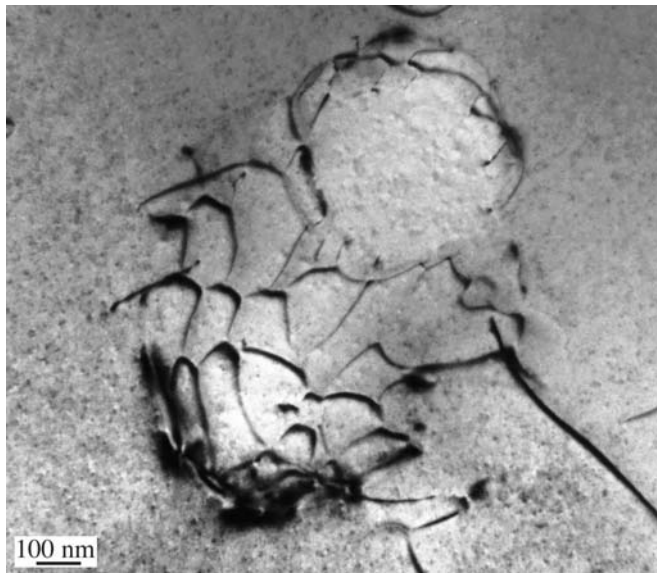

FIGURE 26.24. An irregular array of misfit dislocations at the interface between a spinel particle and a NiO matrix. The lattice mismatch is very small as you can appreciate from the scale. Although you can 'see' a distorted hexagonal array of dislocations, you have to remember that this interface is actually curving within the specimen so that we are only seeing a projection of the structure.

The TEM beam 'sees' yet another change: the extinction distance is different. The result is that, if the crystal is inclined to the electron beam, you will see thickness fringes associated with the interface. Not much work has been done on this, but you may find that it is more difficult to use the **g**.**b** criterion for determining Burgers vectors, especially when the misfit is large.

GB VERSUS PB

This means that the strain field at phase boundaries is *not* the same as at a GB.

Phase transformations often involve the movement of dislocations, generally at semicoherent interfaces. All the conditions discussed above may hold; however, now the dislocations will certainly be associated with a step on the interface to allow the transformation to proceed, so as to physically translate the interface. However, you'll find it difficult to model the contrast from such dislocations, especially when you have a thin layer of the new phase enclosed by the matrix, as is the case when a precipitate grows, as illustrated in Figure 26.25.

The main effect of steps on such interfaces is that they cause a shift in the thickness fringes. It is often difficult to tell if there is also a dislocation present.

We'll summarize some features you should remember when studying dislocations in interfaces

- If the orientation of the grains is different, the distribution of strain from the dislocation may be different in the two grains; the diffraction contrast is determined by this strain field.
- If the chemistry of the two grains is different or if you use different but equal **g** vectors, the extinction distances will be different and the image of the dislocations must therefore be affected.
- Be careful not to confuse moiré fringes with dislocations (we discussed moiré fringes in Chapter 23). The guide is that the dark and light moiré fringes have approximately equal widths; if there is any ambiguity, you should use weak-beam imaging (Chapter 27) and carefully examine the DP.

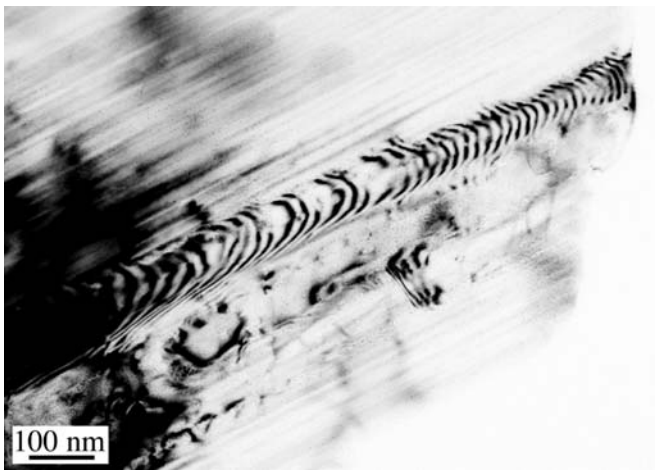

FIGURE 26.25. Transformation dislocations in the interface between a growing lath of hematite (pseudo-hexagonal alumina structure) in a ferrite (cubic spinel structure) matrix. The dislocations are curved because they were moving while heating the thinned specimen, which is why we know they are transformation dislocations, not simply misfit dislocations.

Humble and Forwood have shown using computer simulation of dislocations in interfaces that it is best to use diffraction conditions where a reflection is satisfied in both grains, otherwise the dislocation images tend to be rather featureless relative to the interface thickness fringes.

26.10 VOLUME DEFECTS AND PARTICLES

When the defects are small, the image may be dominated by the strain-field contrast; that is the aspect we are considering here. You have to remember, though, that these defects may have a different structure, lattice parameter, and composition. The theory for a spherical particle in a matrix was given over 40 years ago and is known as Ashby-Brown contrast. The theory works well for coherent particles but as soon as the first interface dislocation forms, analysis becomes much more difficult.

Lattice-strain effects around spherical precipitates appear as lobes of low intensity with a line of no contrast perpendicular to **g**, as shown schematically in Figure 26.26. If you measure the size of the precipitates from a DF image and the size of the strain-contrast lobes in BF, you can get a direct measure of the lattice strain surrounding a single precipitate, which is really quite remarkable. The process requires some specific experimental conditions and careful calibration of the image recording procedure. It is quite a specialized study, so you should read the original references for details. If your precipitates aren't spherical, intuitive interpretation of the images is unreliable and you have to resort to computer simulation.

Figure 26.26B shows how a spherical particle might strain the lattice. Notice that in this case, all the planes continue across the particle so it is coherent and there are no misfit dislocations. The figure here assumes that all the strain occurs in the matrix, which is only true for a hard particle in a soft matrix. The displacement field used to model this situation is

$$\mathbf{R} = C_\varepsilon \mathbf{r} \tag{26.14}$$

when $\mathbf{r} \leq \mathbf{r}_0$, and

$$\mathbf{R} = C_\varepsilon \frac{r_0^3}{r^3}\mathbf{r} \tag{26.15}$$

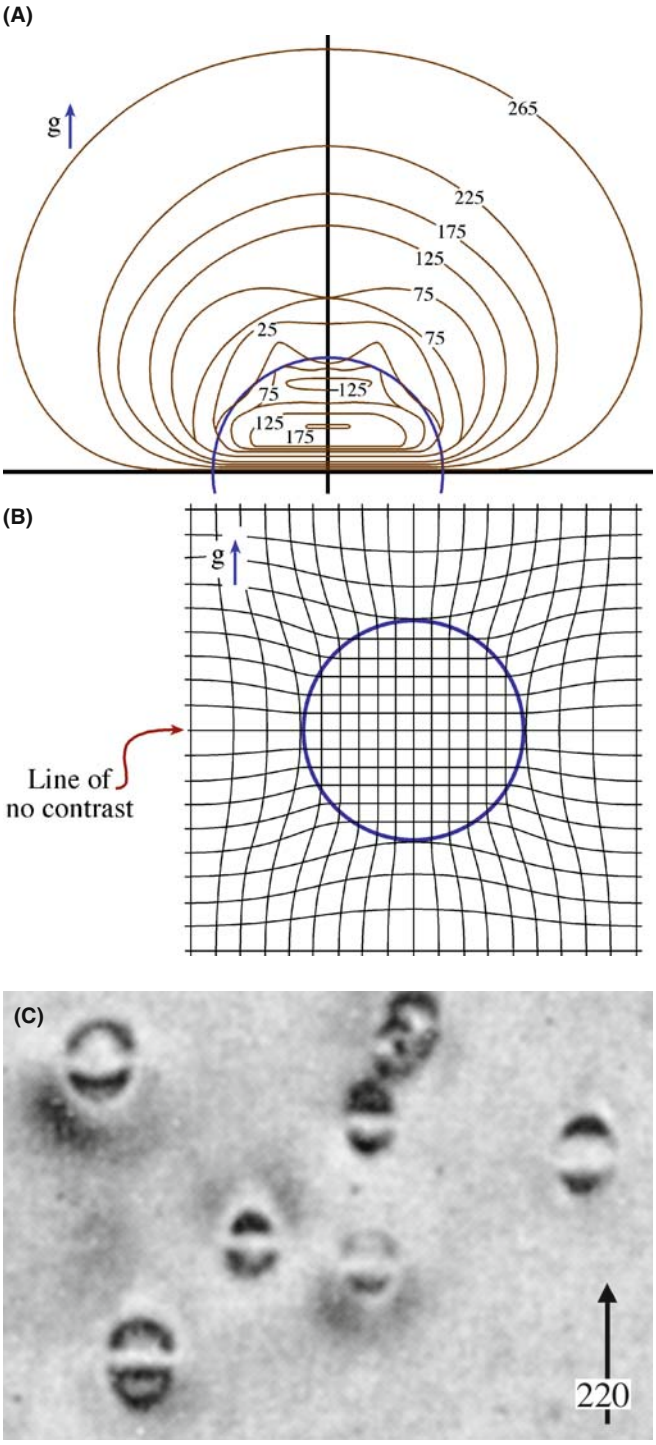

FIGURE 26.26. (A) Intensity contours from a simulated image of a particle like that shown schematically in (B). Notice the line of no contrast which corresponds to the plane which is not distorted by the strain field of the particle. (C) Experimental image of coherent particles in Cu-Co showing strain contrast and a line of no contrast as predicted.

when $\mathbf{r} \geq \mathbf{r}_0$. C_ε is an expression for the elastic constants, given by

$$C_\varepsilon = \frac{3K\delta}{3K + 2E(1+\nu)} \qquad (26.16)$$

K is the bulk modulus of the precipitate; E and ν are Young's modulus and Poisson's ratio, respectively, for the matrix. The important feature is that $\mathbf{R}$ always has radial symmetry. Thus, when we consider the Howie-Whelan equations, we realize that when $\mathbf{g}.\mathbf{R} = 0$ we will see no contrast. So, there will be a 'line of no contrast' normal to $\mathbf{g}$.

The strain can be plotted using the equations given by Ashby and Brown and the image simulated (see below), as shown in Figure 26.26A. In the image from a specimen of a Cu-Co alloy containing small Co precipitates shown in Figure 26.26C, we can see that the images of the particles resemble butterflies or coffee beans. With the improvement in computers, the image contrast expected from much more complex particle geometries can now be calculated and can even consider statistical structural fluctuations.

26.11 SIMULATING IMAGES

It is important that you understand the origins of diffraction contrast from strain fields before you try to simulate this contrast using a computer. Having said that, few students would want to calculate image intensities by hand. The Howie-Whelan equations can be used to simulate images of dislocations, which is especially important when the dislocations are close together. The principal approaches used to simulate diffraction-contrast images were discussed in Sections 25.11–25.13.

Although the algorithm employed by the Head et al. programs allows very fast computation of the image, it does so by restricting the geometry of the defects. To cope with more general geometries, e.g., the strain field from end-on screw dislocations or non-parallel dislocations, we can use Thölén's matrix algorithm. As we saw in Chapter 25, the Howie-Basinski treatment extends the two-beam calculations to include several beams on the systematic row and provides a method for circumventing the column approximation.

PHOTOGRAPHIC FILM

If you want to make quantitative comparisons with real images on film, you must correct for the non-linearity of the film (see Chapters 30 and 31).

26.11.A The Defect Geometry

When choosing the optimal simulation method, depending on the defect geometry, the problem of calculating the image belongs to one of three categories

- *Two-dimensional problem*: including the most general geometries where integration of the full two-dimensional (x,y) grid is necessary.
- *One-dimensional problem*: geometries where the image depends only on either x or y and can be represented by a profile, e.g., problems involving a dislocation parallel to the foil surfaces.
- *GCS problem*: geometries where the method of generalized cross sections (GCS), developed by Head et al., can be applied. Situations where the dislocations and fault planes are parallel to each other, but inclined to the foil surface, are included in this group.

Choosing the best method can speed up the simulations considerably, as we'll show later. The Head et al. program automatically determines the category and selects the appropriate calculation method.

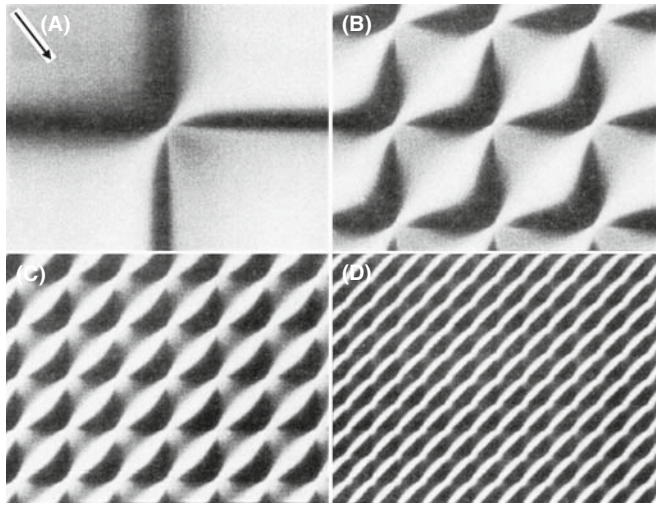

FIGURE 26.27. Comis simulations of two-beam BF images of networks of screw dislocations, located in the middle of a foil with thickness equal to four times the extinction distance, $\xi_{\mathbf{g}}$; $\mathbf{g}.\mathbf{b} = 1$ for both dislocation types. The separation between the dislocations is (A) ∞, (B) $1\xi_{\mathbf{g}}$, (C) $0.5\xi_{\mathbf{g}}$, (D) $0.25\xi_{\mathbf{g}}$.

26.11.B Crystal Defects and Calculating the Displacement Field

The program Comis could simulate amplitude contrast from any number of defects consisting of fault planes and straight, infinite dislocations. You just needed to define the Burgers vector, line direction, and relative position; planar faults were defined by the plane normal, the displacement vector, and the relative position. You could then predefine certain standard geometries to ease the process of defining the defect system.

Once you've defined the defect geometry, you must consider the region of the crystal you want to simulate. In situations where the 'interesting' region is well defined (as in the case of inclined dislocations or intersecting dislocations), Comis determined this region and provided it as the default. However, you could always set the image region manually in Ångström units, to obtain a desired magnification.

The displacement field for the dislocations was calculated in Comis using linear, anisotropic elasticity theory and was based on the algorithms of Head et al., so you had to specify the elastic constants of your crystal. The displacement field then corresponds to straight, infinite dislocations in an infinite medium with no account taken of surface relaxations. In any simulation, you should be able to introduce image dislocations outside the crystal in order to include surface effects.

26.11.C The Parameters

An example which shows simulated images of an orthogonal network of screw dislocations is given in Figure 26.27. Comis could calculate the equilibrium configuration of certain types of interacting dislocations using anisotropic elasticity theory, and then directly incorporates the resulting geometry in subsequent image simulations. As you can appreciate from equation 26.5, in such simulation studies, you will need *all* the parameters for the defects, the specimen, and the diffraction conditions

- The foil thickness.
- The stacking-fault energy.
- The absorption parameters, usually using $|U'_{\mathbf{g}}|/|U_{\mathbf{g}}| = 0.1$.
- The number of beams included in the calculation.
- The zone-axis and the diffracting vectors.
- Also required are the electron energy, the elastic constants, the normal to the foil surface, the Burgers vectors, and the line direction of the dislocations.

The exact beam direction can then be specified by defining the 'center' of the Laue zone, giving the coordinates in terms of the $\mathbf{g}$ vector and $\mathbf{g}_z$. Here $\mathbf{g}_z$ is a specially defined vector in reciprocal space, which is automatically set to lie in the ZOLZ and to be perpendicular to $\mathbf{g}$. Thus, if you place the center of the ZOLZ at (0,0), the specimen is oriented on the zone-axis; if you place the center of the ZOLZ at (0.5,0), it corresponds to being at $\mathbf{g}/2$, i.e., at the Bragg position with the $\mathbf{0}$ and $\mathbf{g}$ beams excited. If you change the second coordinate to be, say, (0.5,0.5), you would include beams from off the systematic row.

CHAPTER SUMMARY

The central idea of this chapter is that the strain field moves atoms off their perfect-crystal positions. We've concentrated on dislocations because the edge dislocation gives the clearest illustration of how the deformation produces the contrast and its structure can be understood with a two-dimensional projection. We can summarize the topics of the chapter as follows

- There is a new feature to the column approximation. The displacement moves atoms out of the column and brings others into the column.
- The basis of the **g**.**b** analysis of a dislocation is simply that the contrast is determined by **g**.**R**(**r**) and that **R**(**r**) is linearly related to **b**. For the screw dislocation, **R**(**r**) is directly proportional to **b**. For the edge dislocation, the image can also be affected by a $\mathbf{g}.\mathbf{b} \times \mathbf{u}$ component which is caused by the buckling of the dislocation glide plane.
- Dislocation images are usually asymmetric. The contrast depends on the sign of $(\mathbf{g}.\mathbf{b})s$.
- As a practical rule, we usually set s to be >0. Then the distortion due to the defect will bend the near-diffracting planes back into the Bragg-diffracting condition to give strong contrast. When $s > 0$, detail in the image is more localized relative to the defect than if we use the $s = 0$ condition.

There are many other situations which are closely related to the topics we've discussed in this chapter. For example, we have not discussed strain contrast associated with crack tips or the analysis of buckling of thin specimens. Although these are rather specialized situations, they do illustrate the growing applications of diffraction contrast in the TEM.

REFERENCES

The text by Hirsch et al. summarizes the early work by the Cambridge group including the derivation of equation 26.10.

BACKGROUND TO DISLOCATIONS AND INTERFACES

Amelinckx, S 1964 *The Direct Observation of Dislocations*, Academic Press New York. A fascinating summary of the early studies by TEM by the man who influenced many. Source of Figure 26.16.

Amelinckx, S 1979 in *Dislocations in Solids* 2, (Ed. FRN Nabarro), North-Holland New York. If you're interested in dislocations, there are many other volumes in this set.

Eshelby, JD, Read WT and Shockley W 1953 *Anisotropic Elasticity with Applications to Dislocation Theory* Acta Metall. **1**, 251–9. An early paper on anisotropic elasticity theory (used by Comis).

Hirth, JP and Lothe, J 1982 *Theory of Dislocations*, 2nd Ed., John Wiley & Sons New York. The definitive textbook, but not for the beginner. Source for equation 26.8, buckling of the glide plane, etc. Not a TEM book.

Hull, D. and Bacon, DJ 2001 *Introduction to Dislocations*, 4th Ed., Pergamon Press New York. A great introductory text.

Matthews, JW, Ed. 1975 *Epitaxial Growth*, Parts A and B, Academic Press New York. Our hero. Unfortunate grammar in the title.

Nabarro, FRN 1987 *Theory of Dislocations*, Dover Publications New York.

Porter, DA and Easterling, KE 1992 *Phase Transformations in Metals and Alloys*, 2nd Ed., Chapman and Hall New York.

Smallman, RE 1985 *Modern Physical Metallurgy*, 4th Ed., Butterworth-Heinemann Boston.

Steeds, JW 1973 *Anisotropic Elastic Theory of Dislocations*, Clarendon Press Oxford, UK. As readable as this subject can be: written by a microscopist. See also Eshelby et al.

Sutton, AP and Balluffi, RW 1995 *Interfaces in Crystalline Materials*, Oxford University Press New York.

Wolf, D and Yip, S, Eds. 1992 *Materials Interfaces, Atomic-level Structure and Properties*. Chapman and Hall New York. A collection of review articles.

IMAGE SIMULATION

Head, AK, Humble P, Clarebrough LM, Morton AJ and Forwood, CT 1973 *Computed Electron Micrographs and Defect Identification* North-Holland New York.

Morton, AJ and Forwood CT 1973 *Equilibria of Extended Dislocations* Cryst. Lattice Defects **4** 165–177. TEM of arrays of interacting dislocations (Section 26.11.C).

Humble, P and Forwood, CT 1975 *Identification of Grain Boundary Dislocations I and II* Phil. Mag. **31**, 1011–23 and 1025–48. Simulating images of interfaces.

Rasmussen, DR and Carter, CB 1991 *A Computer Program for Many-Beam Image Simulation of Amplitude-Contrast Images* J. Electron Microsc. Techniques **18**, 429. Description of Comis, a great program that died with the advances in operating systems.

Thölén, AR 1970a *Rapid Method for Obtaining Electron Microscope Contrast Maps of Various Lattice Defects* Phil. Mag. **22** 175–182. Matrix algorithm for more complex geometries.

Thölén, AR 1970b *On the Ambiguity between Moiré Fringes and the Electron Diffraction Contrast from Closely Spaced dislocations* Phys. stat. sol. *(a)* **2** 537–550. Applying the algorithm to a network of orthogonal dislocations (Section 26.11.C).

Thölén, AR and Taftø, J 1993 *Periodic Buckling of the Lattice Planes in the Thin Regions of Wedge-Shaped Crystals* Ultramicrosc. **48** 27–35. TEM of buckled specimens: challenging exercise.

CONTRAST THEORY

Amelinckx, S 1992 in *Electron Microscopy in Materials Science*, (Eds PG Merli and MV Antisari), World Scientific River Edge NJ. Includes discussion of dislocation strain field relaxing at the surface.

Amelinckx, S and Van Dyck, D 1992 in *Electron Diffraction Techniques* **2** (Ed. J.M. Cowley), p. 1, Oxford University Press New York.

Ashby, MF and Brown, LM 1963 *Diffraction Contrast from Spherically Symmetrical Coherency Strain* Phil. Mag. **8** 1083–1103 and *On Diffraction Contrast from Inclusions* Phil. Mag. **8** 1649-1676. Ashby-Brown contrast.

de Graef, M and Clarke, DR 1993 *Strain Contrast at Crack Tips for in-situ Transmission Electron Microscopy Straining Experiments* Ultramicrosc. **49**, 354–365. TEM of crack tips: challenging exercise.

Goringe, MJ 1975 in *Electron Microscopy in Materials Science* (Eds. U Valdré and E Ruedl), p. 555, Commission of the European Communities Luxembourg. Further discussion of equation 26.10 and much more.

Hirsch, PB, Howie, A and Whelan, MJ 1960 *Kinematical Theory of Diffraction Contrast of Electron Transmission Microscope Images of Dislocations and Other Defects* Phil Trans Roy Soc. **A252** 499–529. Early paper you should read, with more on the column approximation.

The original series of papers by H Hashimoto, PB Hirsch, A Howie, MJ Whelan in Proc. Roy. Soc. London A **252** 499 (1960), **263** 217 (1960), **267** 206 (1962), and **268** 80 (1962) are strongly recommended.

ON THE NON-COLUMN APPROXIMATION

Howie, A and Basinski ZS 1968 *Approximations of the Dynamical Theory of Diffraction Contrast* Phil. Mag. **17** 1039–1063.

Howie, A and Sworn H 1970 *Column Approximation Effects in High Resolution Electron Microscopy using Weak Diffracted Beams* Phil. Mag. **31** 861–864.

EXAMPLES

Hughes, DA and Hansen, N 1995 *High Angle Boundaries and Orientation Distributions at Large Strains* Scripta Met. Mater. **33** 315–321. Particularly clear illustration of the value of producing a large specimen area.

Karth, S, Krumhansl, JA, Sethna, JP and Wickham, LK 1995 *Disorder-Driven Pretransitional Tweed Pattern in Martensitic Transformations* Phys. Rev. B **52** 803–822. Early work considering statistical structural fluctuations on image contrast (in Section 26.10).

Takayanagi, K, Tanishiro, Y, Yagi, K, Kobayashi, K and Honjo, G 1988 *UHV-TEM Study on the Reconstructed Surface of Au(111): Metastable* $p'' \times p''$ *and Stable* $p \times 1$ *Surface Structure* Surf. Sci. **205** 637–651. They showed surface dislocations by TEM before they were discovered by STM.

Tunstall, WJ, Hirsch, PB and Steeds, JW 1964 *Effects of Surface Stress Relaxation on Electron Microscope Images of Dislocations Normal to Thin Metal Foils* Phil. Mag. **9** 99–119. Classic paper on the contrast seen when a screw dislocation intersects a surface.

Wilkens, M 1978 in *Diffraction and Imaging Techniques in Materials Science*, 2nd Ed. (Eds S Amelinckx, R Gevers and J Van Landuyt) p.185 North-Holland New York. A detailed analysis of butterflies, lozenges and peanuts (Figure 26.12).

THE COMPANION TEXT

The programs TEMACI and Cufours are available for simulating these defects. TEMACI was designed for the study of small defects.

SELF-ASSESSMENT QUESTIONS

Q26.1 Give the physical reason for the change in contrast near a dislocation.
Q26.2 We are given an assignment to perform a computer simulation of contrast due to defects. The assignment includes areas of a hypothetical specimen with dimensions of about 1 nm. Is the column approximation valid?
Q26.3 A screw dislocation in your specimen appears to be out-of-contrast. Does this mean $\mathbf{g}.\mathbf{R}=0$?
Q26.4 An edge dislocation has $\mathbf{g}.\mathbf{b} = 0$ but it still shows strong contrast. Why?
Q26.5 Is the image of a dislocation located directly at the projected position of the dislocation?
Q26.6 Is the information in the image of dislocation core located coming from the reflection **g**?
Q26.7 You are looking at a region in the image that is about 1 μm in diameter. Could this be the strain field from a defect?
Q26.8 You see abrupt steps in the thickness fringes at different locations in the specimen. What might cause this?
Q26.9 How can you 'see' a dislocation and why do we use quotes in this question?
Q26.10 What parameters are needed to describe a particular dislocation?
Q26.11 How do we determine the Burgers vector of a dislocation?
Q26.12 How is the Burgers vector determined for dislocation nodes or networks?
Q26.13 What complications arise for small dislocation loops?
Q26.14 Why do dislocation dipoles show 'inside-outside' contrast?
Q26.15 What happens to $\mathbf{g}.\mathbf{b}$ dislocation contrast when **g** is reversed?
Q26.16 How does using a higher kV help in 'viewing' dislocations?
Q26.17 How does using a lower kV help in 'viewing' dislocations?
Q26.18 Give two ways that the surface can affect the image of a dislocation.
Q26.19 Why do we talk about $\mathbf{g}.\mathbf{b}$ rather than $\mathbf{g}.\mathbf{R}$?
Q26.20 How does the term $\mathbf{g}.\mathbf{b}\times\mathbf{u}$ relate to $\mathbf{g}.\mathbf{R}$?

TEXT-SPECIFIC QUESTIONS

T26.1 Consider Figure 26.1A. How wide do you expect the dislocation image (the peak in 'B') to be? Just give your thought process without doing displacement-field calculations, etc.
T26.2 Consider Figure 26.3. Why do we always like to have **b** lying in the plane of the specimen? (Give at least three different valid reasons.)
T26.3 Figure 26.5 suggests that if we keep $\mathbf{g}.\mathbf{b}$ the same but reverse the sign of s, the image of the dislocation will arise from the other side of the dislocation core. Use your analysis of the Howie-Whelan equations to explain this result.
T26.4 Give a physical explanation of equation 26.12 and discuss how it differs from using **R**.
T26.5 Consider Figure 26.6A. Give a consistent set of **b** vectors for all the dislocations you see.
T26.6 Consider Figure 26.6C. By consulting the original source or otherwise, explain the variation in the separation of the dislocation images.
T26.7 Consider the lower half of Figure 26.6G,H. Explain why all the dislocations are visible in the two **g** vectors.
T26.8 Consider Figure 26.8. Suggest a set of consistent **g** vectors for the four images.
T26.9 Consider Figure 26.10. Why are the fringes on one loop running in a different direction? Suggest what **g** might be and include it on the diagram.
T26.10 Consider Figure 26.11. Explain how $\mathbf{g}.\mathbf{b}\times\mathbf{u}$ can lie in the plane of the loop and thus confirm the interpretation of the contrast in this image.
T26.11 Consider Figure 26.16A and B. Estimate the angle through which the specimens bend.
T26.12 How can we increase the information on dislocations parallel to the specimen surface if dislocations with values of $\mathbf{g}.\mathbf{b}$ which are <0.3 can't be distinguished from those with $\mathbf{g}.\mathbf{b} = 0$?